

Renormalization group improved m_s and $|V_{us}|$ determination from hadronic τ decays.

B. Ananthanarayan,^{1,*} Diganta Das,^{2,†} and M. S. A. Alam Khan^{1,‡}

¹*Centre for High Energy Physics, Indian Institute of Science, Bangalore 560 012, India*

²*Center for Computational Natural Sciences and Bioinformatics,
International Institute of Information Technology, Hyderabad 500 032, India*

We determine the strange quark mass (m_s) and quark mixing element $|V_{us}|$, and their joint determination from the Cabibbo suppressed hadronic τ decays in various perturbative schemes. We have improved this analysis compared to the previous analysis based on the optimal renormalization or the renormalization group summed perturbation theory (RGSPT) scheme, by replacing the theoretical longitudinal contributions with phenomenological parametrization, and the RGSPT coefficients are used for the dimension-4 Adler functions. The improved analysis results in the extraction of $m_s(2\text{ GeV}) = 98 \pm 19\text{ MeV}$ and $|V_{us}| = 0.2191 \pm 0.0043$ from the RGSPT scheme.

I. INTRODUCTION

The hadronic decays of the τ leptons have been of constant interest for determining various parameters of the Standard Model (SM) of particle physics. The availability of experimental data on the strange and non-strange decay modes for the hadronic τ decays has opened the window for the determination of various parameters relevant for the quantum chromodynamics (QCD), namely the strong coupling constant α_s , the strange quark mass m_s , the vacuum condensates, the low-energy chiral couplings, and the quark mixing element $|V_{us}|$ of the Cabibbo–Kobayashi–Maskawa (CKM) matrix (see ref. [1, 2] for details).

On the theoretical side, the QCD contributions to the hadronic τ decays are studied by evaluating the current correlator using the Operator Product Expansion (OPE)[3]. The OPE factorizes the long- and short-distance contributions. The long-distance information is encoded into the vacuum condensates. The short distance part is written as the perturbative series in the strong coupling constant and quark masses. The vacuum condensates can also be evaluated using chiral perturbation theory (ChPT) [4], lattice QCD [5], and Renormalization Group (RG) optimized perturbation theory [6, 7]. The short distance contributions require the evaluation of the Feynman diagrams. It is also known that some of the contributions to the hadronic vacuum polarization function are not captured by the OPE, and it is a quark-hadron duality violation. These duality violating terms are parameterized in a model-dependent way and fitted to experimental data and should also be added to the OPE contributions [8].

The longitudinal component of the QCD Adler function, corresponding to the zero angular momentum state, has been calculated to $\mathcal{O}(\alpha_s^4)$ [9–14]. It has poor convergence behavior and raises the question of the method’s applicability in the extraction of strange quark mass.

This problem can be cured by replacing these contributions with their phenomenological input and has been used in ref. [15–19] for m_s and $|V_{us}|$ extractions from the experimental moment data. These improvements have resulted in much better control over the theoretical uncertainties in the m_s and $|V_{us}|$ determinations.

The hadronic τ decays have been extensively studied using various perturbative schemes. These schemes differ in how strong coupling constant and quark masses are evaluated along the contour in the complex plane using their renormalization-group (RG) properties. The most commonly used schemes in the extraction of strange quark mass and CKM matrix element from the Cabibbo suppressed hadronic τ decay are fixed-order perturbation theory (FOPT) and contour-improved perturbation theory (CIPT). For the hadronic τ decays, the FOPT suffers from the problem of large logarithms along the contour in the complex energy plane, and the higher-order spectral moments are very sensitive to scale variations. In the CIPT scheme, direct numerical evaluation of coupling constant and masses along complex contour using their RGE does not suffer from the problem of the large logarithms. However, scale dependence is still the major source of theoretical uncertainties for higher moments.

Recently, the optimal renormalization or RG-summed perturbation theory (RGSPT) has been used by two of us in ref. [20] in the strange quark mass determination. The behavior of polarization and Adler functions in the complex contour was also studied for RGSPT, CIPT, FOPT, and the method of effective charges (MEC) in great detail. However, the numerical impact of the theoretical uncertainties from perturbation series truncation, and scale dependence were excluded. We improve the previous analysis by:

- Including the RGSPT coefficients for dimension-4 Adler functions.
- Replacing the divergent longitudinal perturbative QCD expressions for the Adler function with the phenomenological parametrization used in ref. [15, 17]. This replacement significantly reduces the theoretical uncertainties.
- Performing $|V_{us}|$ as well as the joint m_s and $|V_{us}|$

* anant@iisc.ac.in

† diganta.das@iiit.ac.in

‡ alam.khan1909@gmail.com

determinations for the first time using RGSPT.

- The effects of the variation of the m_s and $|V_{us}|$ with the variation of the moments calculated at different energies ($s_0 < M_\tau^2$) is also included and found to be constituting an important source of uncertainty.
- Using the five-loop QCD β -function and anomalous dimensions for the running of the strong coupling constant and quark masses.

The article is organized as follows: Section II provides a brief overview of the various quantities that are needed for the extraction of m_s and $|V_{us}|$. A short introduction to RGSPT is given in section III. Section IV explains the OPE contributions to the Adler function. The behavior of leading-order mass corrections to the Adler functions in different schemes used in this article is studied in the section V. The higher-order term of the perturbation series becomes very important for the higher moments, and two prescriptions for the truncation of the perturbation series are also defined in this section. In section VI, the phenomenological parametrization of longitudinal contributions is briefly discussed. Then, we move to section VII where strange quark mass is extracted using only the perturbative QCD (pQCD) contributions calculated from OPE. The weighted average results for the $m_s(M_\tau^2)$ extraction using this method in CIPT, FOPT and RGSPT schemes are presented in table IV. The details of uncertainties can be found in the appendix E1. In section VIII the $m_s(M_\tau^2)$ determination using the phenomenological parametrization for the longitudinal component is performed and results are presented in table V. Details of the strange quark mass determinations from moments are presented in the appendix E2. The determination of $|V_{us}|$ using external input for m_s is performed in section IX. The weighted average results using the OPAL and ALEPH data are presented in table VIII and table VI, respectively. The details of determinations from the moments as well as the uncertainties coming from various sources are presented in appendix E3. In section X the joint extraction of m_s and $|V_{us}|$ is performed. We provide a summary and conclusion in section XI. We also provide supplementary inputs needed for this article in the appendix A,B,D,C. Details of m_s and $|V_{us}|$ determinations from moments can be found in appendix E.

II. FORMALISM

An important quantity for the study of hadronic τ decay width[21–23] is the two-point current correlator:

$$\Pi_{\mu\nu,ij}^{V/A}(p^2) \equiv i \int dy e^{ipy} \langle \Omega | T \left\{ J_{\mu,ij}^{V/A}(y) J_{\nu,ij}^{V/A}(0)^\dagger \right\} | \Omega \rangle \quad (1)$$

where $|\Omega\rangle$ denotes the physical vacuum, $J_{\mu,ij}^{V/A}(y) = (\bar{q}_j \gamma_\mu / (\gamma_\mu \gamma_5) q_i)(x)$ is the hadronic vector/axial current, and the indices i and j denote the flavors of light quarks.

The current correlator can be calculated perturbatively using OPE [3] as a power expansion in $1/p$, and the corresponding coefficients of are the operator of that dimension. Purely perturbative corrections appear up to dimension-2 in the OPE expansion, and the long-distance corrections corresponding to the vacuum condensates start from dimension-4.

Using Lorentz decomposition, the current correlator in eq. (1) can be decomposed into the longitudinal and transverse components with angular momentum $J = 0$ and $J = 1$ as:

$$\Pi_{\mu\nu,ij}^{V/A}(p^2) = (p_\mu p_\nu - g_{\mu,\nu}) \Pi_{ij}^{V/A,T}(p^2) + p_\mu p_\nu \Pi_{ij}^{V/A,L}(p^2). \quad (2)$$

The L/T correlators are related to experimentally measurable semi-hadronic τ decay rate (R_τ), defined by:

$$R_\tau \equiv \frac{\Gamma(\tau^- \rightarrow \text{hadrons } \nu_\tau(\gamma))}{\Gamma(\tau^- \rightarrow e^- \nu_\tau(\gamma))} = R_{\tau,V} + R_{\tau,A} + R_{\tau,S}, \quad (3)$$

and it is related to the imaginary part of the current correlators in eq. (2) by:

$$R_\tau(s_0) = 12\pi \int_0^{s_0} \frac{ds}{s_0} \left(1 - \frac{s}{s_0}\right)^2 \times \left[\left(1 + \frac{2s}{s_0}\right) \text{Im}(\Pi^T)(s) + \text{Im}(\Pi^L)(s) \right]. \quad (4)$$

It should be noted that these current correlators also carry the information about mixing among the quark flavors and can be written as:

$$\Pi^J \equiv \sum_{i=d,s} |V_{ui}|^2 \left[\Pi_{ui}^{V,J}(s) + \Pi_{ui}^{A,J}(s) \right], \quad (5)$$

and $|V_{ij}|$ are the elements of the CKM matrix.

To study the invariant mass distribution of final-state hadrons, we need moments from the hadronic τ decay rate, defined by[24]:

$$R_\tau^{kl}(s_0) \equiv \int_0^{s_0} ds \left(1 - \frac{s}{s_0}\right)^k \left(\frac{s}{s_0}\right)^l \frac{dR_\tau}{ds}, \quad (6)$$

Using integration by parts, we can convert eq. (6) into the following form:

$$R_\tau^{kl}(s_0) = -i\pi \oint_{|x_c|=1} \frac{dx_c}{x_c} \times \left\{ 3\mathcal{F}_{kl}^{L+T}(x_c) \mathcal{D}^{L+T}(s_0 x_c) + 4\mathcal{F}_{kl}^L(x_c) \mathcal{D}^L(s_0 x_c) \right\}, \quad (7)$$

where $x_c = s/s_0$ and $\mathcal{D}^{L+T}(s)$ are the Adler functions.

Usually, the experimental value of the moments defined above are provided for $s_0 = M_\tau^2$ in the literature. However, their values at different energy can be calculated using the experimental data on the spectral functions provided in the refs. [25–28].

(k, l)	$\mathcal{F}_{L+T}^{kl}(x)$	$\mathcal{F}_L^{kl}(x)$
(0,0)	$(1-x)^3(1+x)$	$(1-x)^3$
(1,0)	$\frac{1}{10}(1-x)^4(7+8x)$	$\frac{3}{5}(1-x)^4$
(2,0)	$\frac{2}{15}(1-x)^5(4+5x)$	$\frac{3}{5}(1-x)^5$
(3,0)	$\frac{1}{7}(1-x)^6(3+4x)$	$\frac{3}{7}(1-x)^6$
(4,0)	$\frac{1}{14}(1-x)^7(5+7x)$	$\frac{3}{7}(1-x)^7$

TABLE I: Kinematic kernels used in this article.

The Adler function satisfies the homogeneous renormalization group equation (RGE) and is related to the current correlators by the relation:

$$\mathcal{D}^{L+T}(s) \equiv -s \frac{d}{ds} (\Pi^{L+T}(s)), \quad (8)$$

$$\mathcal{D}^L(s) \equiv \frac{s}{M_\tau^2} \frac{d}{ds} (s \Pi^L(s)). \quad (9)$$

The resulting quantity in eq. (7) is an expansion in the strong coupling constant, quark masses, and condensates of higher dimension operators. It explicitly depends on the CKM matrix element and the electroweak corrections. These terms are not shown in eq. (7) but factored out in eq. (12) and eq. (13). The kinematic kernels $\mathcal{F}_{L+T}^{kl}(x_c)$ and $\mathcal{F}_L^{kl}(x_c)$ appearing in the eq. (7) are given by:

$$\mathcal{F}_{L+T}^{kl}(x_c) \equiv 2(1-x_c)^{3+k} \sum_{n=0}^l \frac{l!}{(l-n)!n!} (x_c-1)^n \times \frac{(6+k+n) + 2(3+k+n)x_c}{(3+k+n)(4+k+n)}, \quad (10)$$

$$\mathcal{F}_L^{kl}(x_c) \equiv 3(1-x_c)^{3+k} \sum_{n=0}^l \frac{l!}{(l-n)!n!} \frac{(x_c-1)^n}{(3+k+n)}, \quad (11)$$

and their explicit form used in this article is presented in the table I.

Performing the contour integral defined in eq. (7), we can write R_τ^{kl} [21] as:

$$R_\tau^{kl}(s_0) = 3(|V_{ud}|^2 + |V_{us}|^2) S_{EW} \left\{ 1 + \delta'_{EW} + \delta^{(0),kl} + \sum_{n=2,4,\dots} \left(\cos^2(\theta_C) \delta_{ud}^{(n),kl} + \sin^2(\theta_C) \delta_{us}^{(n),kl} \right) \right\}, \quad (12)$$

where $\theta_C = \sin^{-1} \left(|V_{us}| / \sqrt{(|V_{us}|^2 + |V_{ud}|^2)} \right)$ is the Cabibbo angle, $\delta_{ud,us}^{(n)}$ [21] carry the information of contour integrals evaluated in eq. (7), $\delta'_{EW} = 0.0010$ and $S_{EW} = 1.0201 \pm 0.0003$ are one-loop RG-improved electroweak corrections [29, 30].

The most important quantity of interest in the determination of the strange quark mass is the $SU(3)$ breaking

terms $\delta R_\tau^{kl}(s_0)$ [31] defined as

$$\delta R_\tau^{kl}(s_0) \equiv \frac{R_{\tau,V+A}^{kl}(s_0)}{|V_{ud}|^2} - \frac{R_{\tau,S}^{kl}(s_0)}{|V_{us}|^2} \quad (13)$$

$$= 3S_{EW} \sum_{n \geq 2} \left(\delta_{ud}^{(n),kl} - \delta_{us}^{(n),kl} \right), \quad (14)$$

which is free from instanton and renormalon contributions and vanishes in the chiral limit. It is an experimentally measurable quantity that is used as input from table II along with the theoretical quantities appearing in eq. (13) in the strange quark mass determination.

The value of strong coupling constant $\alpha_s(M_Z^2) = 0.1179 \pm 0.0010$ has been taken from ref. [32] and evolved to τ lepton mass scale using five-loop β -function using package REvolver [33]. Its value at τ lepton mass is $\alpha_s(M_\tau^2) = 0.3187 \pm 0.0083$ and has been used in this article.

III. REVIEW OF OPTIMAL RENORMALIZATION

The optimal renormalization technique is used to resum the running logarithms present in the perturbation series using RGE[34–36]. The resulting summed series shows reduced scale dependence and hence a reduction in the theoretical uncertainty in the extraction of a quantity of interest. In the case of hadronic τ decays, where weighted integrals along the complex contour are involved, these running logarithms become very important. Their summation is necessary to perform the perturbative analysis properly. RGSP resums these logarithms, and the resulting fixed order truncated series has less sensitivity to scale variations even for higher moments than FOPT and CIPT.

The perturbative series describing a QCD process is given by:

$$W(x, m) = x^{n_1} m^{n_2} \sum_{i=0} x^i L^j T_{i,j}, \quad (15)$$

where $x \equiv x(\mu^2)$, $L \equiv \log(\mu^2/q^2)$ and $m = m(\mu^2)$. We can rewrite the series as follows:

$$W^{RG\Sigma} = x^{n_1} m^{n_2} \sum_{i=0} x^i S_i[xL], \quad (16)$$

where the $S_i[xL]$ -coefficients are given by:

$$S_i[xL] = \sum_{n=i}^{\infty} T_{n,n-i}(xL)^{n-i}. \quad (17)$$

The RGE for eq. (15) is given by:

$$\mu^2 \frac{d}{d\mu^2} W(x, m) - \gamma_a(x) W(x, m) = 0, \quad (18)$$

$$(\beta(x) \partial_x + \gamma_m(x) \partial_m + \partial_L - \gamma_a(x)) W(x, m) = 0, \quad (19)$$

where $\gamma_a(x) = \sum_{i=0} x^{i+1} \gamma_a^{(i)}$ is the anomalous dimension associated with $W(x, m)$. We can collect the terms corresponding to summed coefficients defined in eq. (17). This process results in a set of coupled differential equations for $S_i[w]$, which can be summarized as:

$$\sum_{i=0}^n \left[\beta_i (\delta_{i,0} + w - 1) S'_{n-i}(w) + S_{n-i}(w) \left(n_2 \gamma_i + \beta_i (n_1 - i + n) + \gamma_a^{(i)} \right) \right] = 0. \quad (20)$$

Here we have substituted $w = 1 - \beta_0 x L$, which simplifies the solutions of differential equations. For further details on RG summation, we refer to ref. [20, 34–39].

The solution to the first three summed coefficients, relevant for dimension-0 and dimension-2 Adler functions, appearing in the eq. (20) can be found in the appendix B. It should be noted that the RGE for dimension-4 operators mix perturbative coefficients with condensates; hence they do not obey eq. (16). The RG-summed perturbative coefficients are relevant for eq. (33) and eq. (34) in the appendix C.

IV. OPE CONTRIBUTIONS TO THE QCD ADLER FUNCTION

A. Leading order contribution

Dimension-zero is the leading perturbative contribution to the current correlator in the massless limit and has been calculated to $\mathcal{O}(\alpha_s^4)$ [40–49]. It receives a contribution only from the transverse piece of the current correlator, which is identical for both vector and axial-vector channels and thus cancels in the eq. (13). The Adler functions obtained using the OPE can be organized as follows:

$$\mathcal{D}^{L+T}(s) = \sum_{n=0,2,4,\dots} \frac{1}{s^{\frac{n}{2}}} \mathcal{D}_n^{L+T}(s), \quad (21)$$

$$\mathcal{D}^L(s) = \frac{1}{M_\tau^2} \sum_{n=2,4,\dots} \frac{1}{s^{\frac{n}{2}-1}} \mathcal{D}_n^L(s), \quad (22)$$

where ij are the flavor indices and the Adler functions in the RHS of the above equations are expansion in α_s , m_q , and the quark and gluon condensate terms. Their definition gets clearer if we take a contour integration along $s = M_\tau^2 e^{i\phi}$ and the coefficient of $(M_\tau^2)^{-n}$ are called operators of dimension $2n$. The massless Adler functions are given by

$$\mathcal{D}_0^{L+T,V/A}(s) = \frac{1}{4\pi} \sum_i x(-s)^i \tilde{K}_i^{L+T}, \quad (23)$$

$$\mathcal{D}_0^{L,V/A}(s) = 0, \quad (24)$$

where $x(-s) = x(q^2) = \alpha_s(q^2)/\pi$ and \tilde{K}_i^{L+T} are the coefficient of Adler function at i^{th} -loop which can be found in appendix D. The RG running of dimension-zero “ $L+T$ ”-component of the Adler function is given by:

$$\mu^2 \frac{d}{d\mu^2} \mathcal{D}_0^{L+T,V/A}(s) = \left(\beta(x) \frac{\partial}{\partial x} + \frac{\partial}{\partial L} \right) \mathcal{D}_0^{L+T,V/A}(s) = 0, \quad (25)$$

where $L = \log(\frac{\mu^2}{s})$, and the QCD beta function ($\beta(x)$) is defined as:

$$\mu^2 \frac{d}{d\mu^2} x(\mu^2) = \beta(x(\mu^2)) = - \sum_i \beta_i x(\mu^2)^{i+2}. \quad (26)$$

The coefficients of the beta function β_i 's are known up to the five-loops and are presented in the appendix A.

B. The Dimension-2 contributions to the Adler Function

The leading order mass corrections to hadronic τ decay rate come from the dimension-2 Adler function. The $\mathcal{D}^{L+T}(s)$ Adler function is known to be $\mathcal{O}(\alpha_s^3)$. [50–55] while \mathcal{D}^L is known to $\mathcal{O}(\alpha_s^4)$ [9–14] and their analytic expression can be found in the appendix D 2. The RG running of dimension-2 operators is given by:

$$\mu^2 \frac{d}{d\mu^2} \mathcal{D}_2^J(s) = \left\{ \frac{\partial}{\partial L} + \beta(x(\mu^2)) \frac{\partial}{\partial x(\mu^2)} + 2\gamma_m(x(\mu^2)) \frac{\partial}{\partial m_i(\mu^2)} \right\} \mathcal{D}_2^J(s) = 0, \quad (27)$$

where the QCD beta function and the quark mass anomalous dimension (γ_m) are known to the five-loop and can be found in the appendix A.

The $SU(3)$ breaking contributions from the Adler function in the determination of quark masses is the difference:

$$\delta \mathcal{D}_2^{J,V+A}(s) \equiv \mathcal{D}_{2,ud}^{J,V+A}(s) - \mathcal{D}_{2,us}^{J,V+A}(s) \quad (28)$$

where $J = (L+T)/L$ and the analytic expressions can be found in the appendix D 2. These contributions are used in eq. (13) to evaluate the leading order mass correction term $\delta_{ud}^{(2),kl} - \delta_{us}^{(2),kl}$.

The absence of a coefficient $\mathcal{O}(\alpha_s^4)$ for the “ $L+T$ ”-Adler function induces an additional theoretical uncertainty in the predictions from the perturbation theory. This missing piece can be estimated by $\tilde{d}_4^{L+T} \sim (\tilde{d}_3^{L+T})^2 / \tilde{d}_2^{L+T} \approx 4067$ and this value is used in the strange quark mass determinations in this article.

The renormalization group running of different coefficients for CIPT and FOPT coefficients can be found in the ref. [22, 56]. The RG-summed coefficients can be obtained from appendix B by setting $\{n_1, n_2\} = \{0, 2\}$.

C. The Dimension-4 contributions to the Adler Function

The OPE expansion at dimension-4 involves contributions from perturbative and quark, and gluon condensates [22, 57]. However, these contributions are suppressed by a factor of $(\frac{1}{M^2})^2$, and they have the following form:

$$\mathcal{D}_{4,ij}^{L+T,V/A}(s) = \frac{1}{s^2} \sum_{n=0} \tilde{\Omega}_n^{L+T}(s) x(-s)^n, \quad (29)$$

$$\mathcal{D}_{4,ij}^{L,V/A}(s) = \frac{1}{M_\tau^2 s} \left\{ \frac{3}{2\pi^2} \sum_{n=0} \tilde{\Omega}_n^L(s) x(-s)^n - \langle (m_i \mp m_j) (\bar{q}_i q_i \mp \bar{q}_j q_j) \rangle \right\}, \quad (30)$$

where the upper/lower sign corresponds to the V/A component. The $\tilde{\Omega}^{L+T/L}$ coefficients are given by:

$$\begin{aligned} \tilde{\Omega}^{L+T}(s) &= \frac{1}{6} \langle G^2 \rangle + 2 \langle m_i \bar{q}_i q_i + m_j \bar{q}_j q_j \rangle \tilde{q}_n^{L+T} \\ &\pm \frac{8}{3} \langle m_j \bar{q}_i q_i + m_i \bar{q}_j q_j \rangle \tilde{t}_n^{L+T} + \sum_k \langle m_k \bar{q}_k q_k \rangle \\ &- \frac{3}{\pi^2} \left\{ (m_i^4 + m_j^4) \tilde{h}_n^{L+T} - m_i^2 m_j^2 \tilde{g}_n^{L+T} \right. \\ &\pm \frac{5}{3} m_i m_j (m_i^2 + m_j^2) \tilde{k}_n^{L+T} + \sum_k m_k^4 \tilde{j}_n^{L+T} \\ &\left. + 2 \sum_{k \neq l} m_k^2 m_l^2 \tilde{u}_n^{L+T} \right\}, \quad (31) \end{aligned}$$

$$\tilde{\Omega}^L(s) = (m_i^2 + m_j^2) \tilde{h}_n^L \pm \frac{3}{2} m_i m_j \tilde{k}^L + \sum_k m_k^2 \tilde{j}_n^L, \quad (32)$$

where $\langle m_i \bar{q}_j q_j \rangle \equiv \langle 0 | m_i \bar{q}_j q_j | 0 \rangle (-\xi^2 s)$, $m_i = m_j (-\xi^2 s)$, $\langle G^2 \rangle \equiv \langle 0 | G^2 | 0 \rangle (-\xi^2 s)$ and ξ is the scale parameter to keep track of the dependence of the renormalization scale. The RG-evolution of the perturbative coefficients and the condensates can be found in the ref. [22].

The relevant OPE corrections to strange quark mass determination are as follows:

$$\begin{aligned} \delta \mathcal{D}_4^{L+T}(s) &\equiv \mathcal{D}_{4,ud}^{L+T,V+A}(s) - \mathcal{D}_{4,us}^{L+T,V+A}(s) \\ &= \frac{-4\delta O_4}{s^2} \sum_{n=0} \tilde{q}_n^{L+T} x(-s)^n + \frac{6}{\pi^2 s^2} m_s (-s)^4 (1 - \epsilon_d^2) \times \\ &\sum_{n=0} \{ (1 + \epsilon_d^2) \tilde{h}_n^{L+T} - \epsilon_u^2 \tilde{g}_n^{L+T} \} x(-s)^n, \quad (33) \end{aligned}$$

$$\begin{aligned} \delta \mathcal{D}_4^L(s) &\equiv \mathcal{D}_{4,ud}^{L,V+A}(s) - \mathcal{D}_{4,us}^{L,V+A}(s) \\ &= \frac{2\delta O_4}{s M_\tau^2} - \frac{3}{\pi^2 s M_\tau^2} m_s^4 (1 - \epsilon_d^2) \times \\ &\sum_{n=0} \{ (1 + \epsilon_d^2) (\tilde{h}_n^L + \tilde{j}_n^L) + \epsilon_u^2 (2\tilde{h}_n^L - 3\tilde{k}_n^L + \tilde{j}_n^L) \} x(-s)^n, \quad (34) \end{aligned}$$

where $\delta O_4 = \langle 0 | m_s \bar{s} s - m_d \bar{d} d | 0 \rangle (-\xi^2 s)$ with $\epsilon_u = m_u/m_s$ and $\epsilon_d = m_d/m_s$. Using the numerical values

$$\begin{aligned} v_s &= 0.738 \pm 0.029 [58], \\ f_\pi &= 92.1 \pm 0.8 \text{ MeV}, \quad m_\pi = 139.6 \text{ MeV} [32] \\ \epsilon_d &= 0.053 \pm 0.002, \quad \epsilon_u = 0.029 \pm 0.003 [59], \quad (35) \end{aligned}$$

δO_4 can be estimated similar to ref. [22] as:

$$\begin{aligned} \delta O_4 &= (v_s m_s - m_d) \langle 0 | \bar{d} d | 0 \rangle \\ &\simeq -\frac{m_s}{2\hat{m}} (v_s - \epsilon_d) f_\pi^2 m_\pi^2 \\ &= -(1.54 \pm .08) \times 10^3 \text{ GeV}^{-4}. \quad (36) \end{aligned}$$

V. THE BEHAVIOR OF LEADING ORDER PERTURBATIVE MASS CORRECTIONS IN DIFFERENT RENORMALIZATION SCHEMES

The FOPT and CIPT are the two versions of perturbative theory for the QCD analysis of the τ decay frequently used in the literature, and it has been further extended by including an RGSPT version of perturbation theory [20, 37]. It has been shown in the ref. [37] that the $\delta^{(0)}$ contributions from the RGSPT scheme approach CIPT at higher orders of the perturbation theory, and the corresponding numerical value of the strong coupling constant lies closer to the CIPT value. Similar behavior is also observed in this article for the higher dimensional operators, but with the advantage that the scale dependence for higher moments is under control in the case of RGSPT compared to the FOPT and CIPT. Before moving on to the strange quark mass determination, the convergence behavior of the leading order mass corrections must be analyzed carefully for different schemes. This exercise is performed in the rest of the section.

The leading order mass corrections to moment $\delta R_\tau^{kl,2}$ in eq. (13) are given by:

$$\delta R^{kl,D=2} = 24 \frac{m_s (\xi^2 M_\tau^2)^2}{M_\tau^2} S_{EW} (1 - \epsilon_d^2) \Delta_{kl}(x, \xi), \quad (37)$$

where,

$$\Delta_{kl}(x, \xi) \equiv \left(\frac{3}{4} \Delta_{kl}^{L+T}(x, \xi) + \frac{1}{4} \Delta_{kl}^L(x, \xi) \right), \quad (38)$$

and the $\Delta_{kl}^J(x, \xi)$ are the contributions from the Adler functions $\delta \mathcal{D}^J$ involving eq. (D5),(D8),(D11)) evaluated along a contour in the complex plane with the kernels presented in table I. These functions are calculated differently in various schemes explained in the later subsections.

It should be noted that the leading-order mass corrections are presented to remember where perturbative series is truncated in prescription I.

A. CIPT scheme

In CIPT, the masses and the strong coupling evolved along the contour in the complex plane by solving the RGE numerically. By construction, it does not suffer from the problem of large logarithm along the contour. Following the ref. [22, 56, 60], dimension-2 contribution to “ $L + T$ ”-component moments can be organized in terms of contour integrals:

$$\Delta_{kl}^{L+T}(x, \xi) = -\frac{1}{4\pi i} \sum_{n=0} \tilde{d}_n^{L+T}(\xi) \oint_{|x_c|=1} \frac{dx_c}{x_c^2} \mathcal{F}_{kl}^{L+T}(x_c) \times \frac{m_s^2(-\xi^2 M_\tau^2 x_c)}{m_s^2(M_\tau^2)} x^n(-\xi^2 M_\tau^2 x_c), \quad (39)$$

and for the longitudinal component:

$$\Delta_{kl}^L(x, \xi) = \frac{1}{2\pi i} \sum_{n=0} \tilde{d}_n^L(\xi) \oint_{|x_c|=1} \frac{dx_c}{x_c} \mathcal{F}_{kl}^L(x_c) \times \frac{m_s^2(-\xi^2 M_\tau^2 x)}{m_s^2(M_\tau^2)} x^n(-\xi^2 M_\tau^2 x), \quad (40)$$

The dimension-2 contributions to Δ_{kl}^{L+T} for $x(M_\tau^2) = 0.3187/\pi$ contributions of different orders are given by:

$$\begin{aligned} \Delta_{0,0}^{L+T} &= \{0.7717, 0.2198, 0.0777, -0.0326, -0.135\}, \\ \Delta_{1,0}^{L+T} &= \{0.9247, 0.3324, 0.1951, 0.0866, -0.0375\}, \\ \Delta_{2,0}^{L+T} &= \{1.0605, 0.4410, 0.3202, 0.2302, 0.1019\}, \\ \Delta_{3,0}^{L+T} &= \{1.1883, 0.5504, 0.4567, 0.4021, 0.2897\}, \\ \Delta_{4,0}^{L+T} &= \{1.3130, 0.6634, 0.6073, 0.6065, 0.5337\}. \end{aligned} \quad (41)$$

which shows good convergence up to $(2, 0)$ -moment. The longitudinal contributions are:

$$\begin{aligned} \Delta_{0,0}^L &= \{1.6031, 1.1990, 1.1583, 1.3023, 1.6245\}, \\ \Delta_{1,0}^L &= \{1.3832, 1.1358, 1.1970, 1.4642, 1.9856\}, \\ \Delta_{2,0}^L &= \{1.2563, 1.1158, 1.2635, 1.6553, 2.4004\}, \\ \Delta_{3,0}^L &= \{1.1783, 1.1204, 1.3494, 1.8740, 2.8757\}, \\ \Delta_{4,0}^L &= \{1.1301, 1.1418, 1.4517, 2.1216, 3.4196\}, \end{aligned} \quad (42)$$

and we can see that longitudinal contributions show divergent behavior. The total perturbative contributions of dimension-2 is obtained using eq. (38) are:

$$\begin{aligned} \Delta_{0,0} &= \{0.9795, 0.4646, 0.3478, 0.3011, 0.3050\}, \\ \Delta_{1,0} &= \{1.0393, 0.5333, 0.4456, 0.4310, 0.4682\}, \\ \Delta_{2,0} &= \{1.1094, 0.6097, 0.5560, 0.5865, 0.6765\}, \\ \Delta_{3,0} &= \{1.1858, 0.6929, 0.6799, 0.7701, 0.9362\}, \\ \Delta_{4,0} &= \{1.2673, 0.7830, 0.8184, 0.9853, 1.2552\}. \end{aligned} \quad (43)$$

It is clear from the eq. (43) that the pathological longitudinal contributions are a restricting factor in getting any reliable determination from CIPT unless we truncate the perturbative series to the minimum term.

B. FOPT scheme

In FOPT, the perturbative series for the Adler function is truncated to a given order in $\alpha_s(\mu)$, and running logarithms are integrated analytically along the contour in the complex energy plane[56, 61]. The Δ_{kl}^J for FOPT is evaluated by inserting eq. (D6),(D9) in eq. (37) and can be written as:

$$\Delta_{kl}^J(x, \xi) = \sum_{i=0}^4 \sum_{j=0}^i x^i (\xi^2 M_\tau^2) \tilde{d}_{i,j}^J H_j^{kl,J}(x, \xi), \quad (44)$$

where $H_i^{kl,J}(\xi)$ are evaluated analytically:

$$H_n^{kl,L+T}(x, \xi) \equiv \frac{-1}{4\pi i} \oint_{|x_c|=1} \frac{dx_c}{x_c^2} \mathcal{F}_{kl}^{L+T}(x_c) \log^n \left(\frac{-\xi^2}{x_c} \right), \quad (45)$$

$$H_n^{kl,L}(x, \xi) \equiv \frac{1}{2\pi i} \oint_{|x_c|=1} \frac{dx_c}{x_c} \mathcal{F}_{kl}^L(x_c) \log^n \left(\frac{-\xi^2}{x_c} \right). \quad (46)$$

Evaluating the above integrals, the Δ_{kl}^{L+T} contribution, using FOPT, at different orders of perturbative series is given by:

$$\begin{aligned} \Delta_{0,0}^{L+T} &= \{1.0000, 0.4058, 0.2575, 0.1544, 0.0163\}, \\ \Delta_{1,0}^{L+T} &= \{1.0000, 0.5072, 0.4168, 0.3679, 0.2971\}, \\ \Delta_{2,0}^{L+T} &= \{1.0000, 0.5782, 0.5366, 0.5414, 0.5429\}, \\ \Delta_{3,0}^{L+T} &= \{1.0000, 0.6323, 0.6330, 0.6892, 0.7636\}, \\ \Delta_{4,0}^{L+T} &= \{1.0000, 0.6758, 0.7140, 0.8189, 0.9654\}. \end{aligned} \quad (47)$$

Δ_{kl}^L are given by:

$$\begin{aligned} \Delta_{0,0}^L &= \{1.0000, 0.9468, 1.1319, 1.3807, 1.7855\}, \\ \Delta_{1,0}^L &= \{0.7500, 0.7482, 0.9442, 1.2183, 1.6559\}, \\ \Delta_{2,0}^L &= \{0.6000, 0.6229, 0.8184, 1.1006, 1.5520\}, \\ \Delta_{3,0}^L &= \{0.5000, 0.5360, 0.7271, 1.0098, 1.4662\}, \\ \Delta_{4,0}^L &= \{0.4286, 0.4718, 0.6570, 0.9371, 1.3937\}. \end{aligned} \quad (48)$$

We can see that the longitudinal piece has a bad convergence in the FOPT scheme. The total contribution Δ_{kl} is:

$$\begin{aligned} \Delta_{0,0} &= \{1.0000, 0.5410, 0.4761, 0.4610, 0.4586\}, \\ \Delta_{1,0} &= \{0.9375, 0.5675, 0.5486, 0.5805, 0.6368\}, \\ \Delta_{2,0} &= \{0.9000, 0.5894, 0.6071, 0.6812, 0.7952\}, \\ \Delta_{3,0} &= \{0.8750, 0.6082, 0.6565, 0.7694, 0.9393\}, \\ \Delta_{4,0} &= \{0.8571, 0.6248, 0.6997, 0.8484, 1.0725\}. \end{aligned} \quad (49)$$

We can see that the convergence behavior of dimension-2 contribution in eq. (49) is not very different from the CIPT scheme in eq. (43).

C. RGSPT Scheme

In Optimal renormalization, masses and coupling are fixed at some renormalization scale, but the RG-summed running logarithms are evolved around the contour. Interestingly, contour integration can be done analytically, similar to FOPT. However, due to the summation of the running logarithms, the resulting perturbative contributions are very much closer to the CIPT numbers and can be seen later in this subsection.

The perturbative series in RGSPT scheme for dimension-2 Adler function has form:

$$\Delta_{kl}^J(x, \xi) = \sum_{i=0}^4 \sum_{n=0}^i \sum_{m=0}^n x^i (\xi^2 M_\tau^2)^i \tilde{T}_{i,n,m}^J K_{n,m}^{kl,J}(x, \xi), \quad (50)$$

which is obtained by inserting eq. (D11) into eq. (37) and the corresponding contour integrals $K_{n,m}^{kl,J}(x, \xi)$ have the following form:

$$K_{n,m}^{kl,L+T}(x, \xi) \equiv \frac{-1}{4\pi i} \oint_{|x_c|=1} \frac{dx_c}{x_c} \mathcal{F}_{kl}^{L+T}(x_c) \times \frac{\log^n(1 - \beta_0 x (\xi^2 M_\tau^2) \log(-\xi^2/x_c))}{(1 - \beta_0 x (\xi^2 M_\tau^2) \log(-\xi^2/x_c))^m}, \quad (51)$$

$$K_{n,m}^{kl,L}(x, \xi) \equiv \frac{1}{2\pi i} \oint_{|x_c|=1} \frac{dx_c}{x_c} \mathcal{F}_{kl}^L(x_c) \times \frac{\log^n(1 - \beta_0 x (\xi^2 M_\tau^2) \log(-\xi^2/x_c))}{(1 - \beta_0 x (\xi^2 M_\tau^2) \log(-\xi^2/x_c))^m}. \quad (52)$$

The $\Delta_{i,0}^{L+T}$ contributions for different moments are given by:

$$\begin{aligned} \Delta_{0,0}^{L+T} &= \{0.8878, 0.2307, 0.0799, -0.0328, -0.1561\}, \\ \Delta_{1,0}^{L+T} &= \{0.9990, 0.3690, 0.2263, 0.1220, -0.0176\}, \\ \Delta_{2,0}^{L+T} &= \{1.0885, 0.4931, 0.3736, 0.2980, 0.1691\}, \\ \Delta_{3,0}^{L+T} &= \{1.1652, 0.6095, 0.5246, 0.4957, 0.4043\}, \\ \Delta_{4,0}^{L+T} &= \{1.2336, 0.7212, 0.6806, 0.7153, 0.6891\}. \end{aligned} \quad (53)$$

and the $\Delta_{i,0}^L$ have the form:

$$\begin{aligned} \Delta_{0,0}^L &= \{1.4048, 1.2210, 1.2280, 1.3899, 1.7560\}, \\ \Delta_{1,0}^L &= \{1.1360, 1.1034, 1.2194, 1.5005, 2.0514\}, \\ \Delta_{2,0}^L &= \{0.9687, 1.0302, 1.2287, 1.6169, 2.3536\}, \\ \Delta_{3,0}^L &= \{0.8538, 0.9808, 1.2477, 1.7375, 2.6655\}, \\ \Delta_{4,0}^L &= \{0.7697, 0.9459, 1.2727, 1.8617, 2.9888\}, \end{aligned} \quad (54)$$

Moments (k,l)	δR_τ^{kl}	
	ALEPH	OPAL
(0,0)	0.374 ± 0.133	0.332 ± 0.10
(1,0)	0.398 ± 0.077	0.326 ± 0.078
(2,0)	0.399 ± 0.053	0.340 ± 0.058
(3,0)	0.396 ± 0.042	0.353 ± 0.046
(4,0)	0.395 ± 0.034	0.367 ± 0.037

TABLE II: Spectral moments from ALEPH [31, 62] and OPAL[27]. OPAL moments are calculated using current value of $|V_{us}| = 0.2243 \pm 0.0008$ quoted in the PDG[32].

and the $\Delta(x)$ behave as:

$$\begin{aligned} \Delta_{0,0} &= \{1.0171, 0.4783, 0.3669, 0.3229, 0.3219\}, \\ \Delta_{1,0} &= \{1.0332, 0.5526, 0.4746, 0.4666, 0.4996\}, \\ \Delta_{2,0} &= \{1.0585, 0.6274, 0.5874, 0.6277, 0.7153\}, \\ \Delta_{3,0} &= \{1.0874, 0.7023, 0.7054, 0.8061, 0.9696\}, \\ \Delta_{4,0} &= \{1.1176, 0.7774, 0.8286, 1.0019, 1.2640\}, \end{aligned} \quad (55)$$

We can see from the numerical values provided in eq. (42), eq. (48) and eq. (54) that the longitudinal contributions have a convergence issue, and it is difficult to get the reliable determinations using them as input. However, the important ingredient in the mass determination is $\Delta_{i,j}$, defined in eq. (38). We can see from the numerical values presented in eq. (43), eq. (49) and eq. (55) that these inputs can be taken in the mass determination if we truncate the perturbation series to the term which gives minimum contribution to it. This minimum term of the perturbative series is taken as the truncation uncertainty. This prescription has already been advocated in ref. [62], and we have termed this procedure of truncation as **prescription I**. Another choice is to use all available terms of the perturbation series coefficients of the Adler function, including the estimate for the unknown $\mathcal{O}(\alpha_s^4)$ term of the “ $L + T$ ”-component of the dimension-2 Adler function and termed as **prescription II**. These prescriptions have some advantages and disadvantages, which will be discussed later.

VI. PHENOMENOLOGICAL CONTRIBUTION TO THE LONGITUDINAL SECTOR

We can see from the section V that although the contributions from the “ $L + T$ ” part of the dimension-2 has a better convergence for CIPT and RGSPT relative to the FOPT, the longitudinal contributions are forcing us to truncate the higher-order terms. These pathological contributions get enhanced for higher moments and restrict one to use only the leading-order term of the perturbation series. This problem is cured by replacing the longitudinal perturbative series contributions with the phenomenological contributions from the chiral perturbation theory [15–19]. These contributions carry significantly less theoretical uncertainty and agree well with

the corresponding pQCD results, as shown in ref. [15]. With these advantages at hand, the strange quark mass determination using the pQCD contribution from the “ $L+T$ ”-component of the Adler function combined with phenomenological contributions for longitudinal contributions in section VIII can be performed.

The relevant quantities of interest for phenomenological contributions to $R_{ij,V/A}^{kl,L}$, the longitudinal component of eq. (7), are vector/axial-vector spectral functions $\rho_{ij}^{V/A}(s)$. They are related by:

$$R_{ij,V/A}^{kl,L} = -24\pi^2 \int_0^1 dx_c (1-x_c)^{2+k} x_c^{l+1} \rho_{ij}^{V/A,L}(M_\tau^2 x_c). \quad (56)$$

The pseudoscalar spectral function receives contributions from pion and kaon mass poles and higher resonances in the strange and non-strange channels. We are using the Maltman and Kambor [16] parametrization of the pseudoscalar spectral function for the us and ud channels in our analysis, which is given by:

$$s^2 \rho_{us}^{A,L}(s) = 2f_K^2 m_K^2 \delta(s - m_K^2) + \sum_{i=1,2} 2f_i^2 M_i^2 B_i(s). \quad (57)$$

Here f_i and M_i are the decay constants and masses of resonances, and $B_i(s)$ is the Briet-Wigner resonance function taking the form:

$$B_i(s) = \frac{1}{\pi} \frac{\Gamma_i M_i}{(s - M_i^2)^2 + \Gamma_i^2 M_i^2}, \quad (58)$$

where Γ_i is the decay width of the resonances. The spectral function for the ud channel is obtained by replacing the kaon terms with the pion in eq. (57). For the resonance contributions to pseudoscalar ud and us channels appearing eq. (57), we have used the following data:

	$\pi(1300)$	$\pi(1800)$	$K(1460)$	$K(1800)$
M_i (MeV)	1300	1810	1482	1830
Γ_i (MeV)	400	215	335	250
f_i (MeV)	2.2 ± 0.46	0.19 ± 0.19	21.4 ± 2.8	4.5 ± 4.5

TABLE III: Masses and decay width are taken from PDG [32] and decay constants from ref. [17].

The vector component of spectral function receives dominant contributions from the scalar channels $K\pi, K\eta$ and $K\eta'$ and the spectral function has the following form[19]:

$$\rho_{uj}^{V,L}(s) = \frac{3\Delta_{K\pi}^2}{32\pi^2} \sum_{i=\{\pi,\eta,\eta'\}} \sigma_{Ki} |F_{Ki}(s)|^2, \quad (59)$$

where $\Delta_{K\pi} \equiv M_K^2 - M_\pi^2$. The phase space factor $\sigma_{Ki}(s)$

are given by:

$$\sigma_{Ki}(s) = \theta(s - (M_K + M_i)^2) \times \sqrt{\left(1 - \frac{(M_K + M_i)^2}{s}\right) \left(1 + \frac{(M_K - M_i)^2}{s}\right)}. \quad (60)$$

The strangeness changing scalar form factors $F_{Ki}(s)$ are defined by:

$$\langle \Omega | \partial^\mu (\bar{s} \gamma_\mu u) | \Omega \rangle \equiv -i \sqrt{\frac{3}{2}} \Delta_{K\pi} F_{K\pi}(s), \quad (61)$$

and can be found in ref. [18]. Detailed discussion on the application of these form factors in the extraction of strange quark mass can be found in the refs. [15, 19].

VII. STRANGE QUARK MASS DETERMINATION FROM PQCD

The strange quark mass determination in this section is based on the method used in refs. [20, 22, 62]. In addition, we have employed different schemes to perform the comparative study. The strange quark mass determination from hadronic τ decays using RGSPT has been performed ref. [20]. However, the uncertainties coming from the truncation of perturbative series and the scale dependence of strange quark masses were neglected. We have improved the previous determination using pQCD inputs by including these uncertainties and the determinations made in the two prescriptions mentioned in section V.

It should be noted that the higher dimensional OPE contributions ($d > 4$) to the Adler functions, which are numerically small [22] and not considered in this analysis. The strange quark mass is determined by supplying experimental and theoretical inputs to eq. (13). The RHS of the equation is provided with theory inputs from dimension-2 contributions eqs. (D5), (D8) and dimension-4 with eqs. (33),(34). These quantities are evaluated along the complex contour in different schemes, as explained in section V. We present our weighted averaged determinations for $m_s(M_\tau^2)$ from different moments in the table IV for different schemes. The details of various sources of uncertainty in the two prescriptions are presented in appendix E 1.

We can see from table IV that the strange quark mass determination from different schemes agrees with each other within uncertainty. It is also evident from the tables presented in appendix E 1 that the uncertainties in the final strange quark mass are higher in prescription I than in prescription II mainly due to the truncation of the perturbative series. We also emphasize that the systematic comparison of the behavior of perturbative series in different schemes can only be made in prescription II, where the same order information is used. The

RGSPPT provides better control over the theoretical uncertainty by minimizing the renormalization scale dependence. The scale dependence of the strange quark mass for various moments is shown in the figure 1, plotted using prescription II. These plots indicate that the strange mass from the RGSPPT scheme is stable for a wider range of scale variations for the moments under consideration. It should be noted that the uncertainties associated with renormalization scale dependence are included only in the range $\xi \in [0.75, 2.0]$ in the strange mass determination in

table IV.

It should be noted that the poor convergence of the longitudinal contributions restricts this method to be applicable in the lower energies $s_0 < M_\tau^2$. Additional uncertainties in the determinations of m_s arise due to the variations of the upper limit of the moment in the integral s_0 defined in eq. (4). These are estimated using the phenomenological determination, discussed in the next section, and are also included in the table IV. Further details on the numerical uncertainties using pQCD inputs can be found in the appendix E 1.

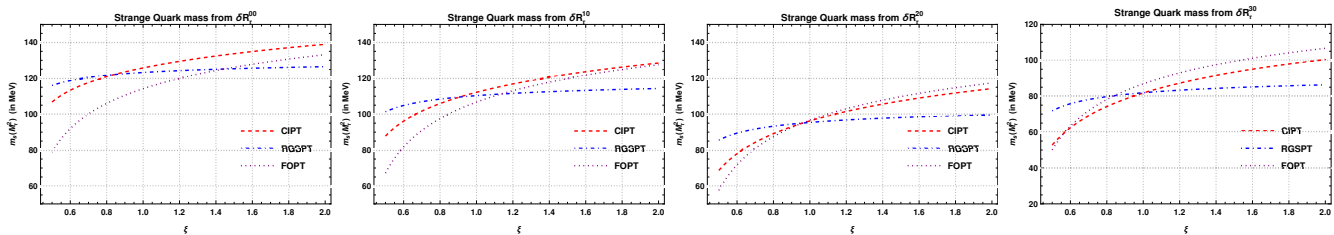


FIG. 1: The scale variation of the strange quark mass in different perturbative schemes using pQCD inputs.

Perturbative Scheme	$m_s(M_\tau^2)$ using prescription I (in MeV)		$m_s(M_\tau^2)$ using prescription II (in MeV)	
	ALEPH	OPAL	ALEPH	OPAL
CIPT	117.7 ± 28.5	105.9 ± 27.5	93.2 ± 24.1	84.1 ± 22.7
FOPT	129.3 ± 33.5	116.2 ± 29.2	94.2 ± 25.4	85.2 ± 23.9
RGSPPT	120.2 ± 23.4	107.7 ± 25.1	89.4 ± 16.4	80.1 ± 15.8

TABLE IV: Weighted average of the strange quark mass in different perturbative schemes.

VIII. STRANGE QUARK MASS DETERMINATION USING PHENOMENOLOGICAL INPUTS

The determination of the strange quark mass in this section is similar to the one used in section VII, but now the longitudinal Adler function is replaced with the phenomenologically parameterized contributions, as discussed in section VI. It should be noted that the “ $L+T$ ” component of the Adler function at dimension-2 is known to $\mathcal{O}(\alpha_s^3)$ and we do not use its estimate for the $\mathcal{O}(\alpha_s^4)$ coefficient in the determination of $m_s(M_\tau^2)$ using phenomenological inputs. Contributions from the last known term of the perturbation series of the Adler function are taken as the total truncation uncertainty, similar to that of the previous section.

Following the discussions of section VI, we now have all the necessary ingredients for the strange quark mass determination. Using the transverse contributions used

in section VII and combining them with the input from section VI, we determine the strange quark in different schemes. We present our result for the weighted average in the table V and the further details of the determinations from moments in the appendix E2. The scale dependence in the $m_s(M_\tau^2)$ is presented in the figure 2 using prescription II. As observed in the previous section, the strange quark mass determinations from the RGSPPT scheme are stable over the wider range of scale variation for moments under consideration. The determination of the m_s from the traditional spectral moments is sensitive to the variation of the s_0 . A typical 5% variation of the s_0 from M_τ^2 in the range $s_0 \in [3, M_\tau^2]$ induces variations of $\sim 6-13\%$ in the m_s determinations from moments using the OPAL data. Unfortunately, such variations can not be calculated for the ALEPH moments as the strange spectral function is not publicly available. These uncertainties are estimated from the determinations using the OPAL data.

Perturbative Scheme	$m_s(M_\tau^2)$ using prescription I (in MeV)		$m_s(M_\tau^2)$ using prescription II (in MeV)	
	ALEPH	OPAL	ALEPH	OPAL
CIPT	123.3 ± 22.3	106.3 ± 21.5	125.1 ± 25.1	107.5 ± 23.9
FOPT	136.6 ± 35.0	119.5 ± 35.4	115.8 ± 30.1	101.6 ± 28.3
RGSPT	123.1 ± 21.1	107.0 ± 21.2	117.7 ± 20.1	102.0 ± 19.5

TABLE V: The weighted average of strange quark mass in the different perturbative schemes. Phenomenological inputs for the longitudinal contributions are used.

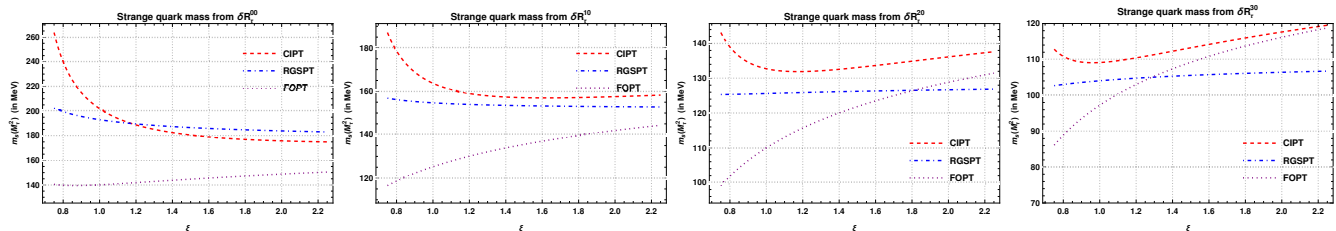


FIG. 2: The scale variation of the strange quark mass obtained from phenomenological inputs in different perturbative schemes.

IX. DETERMINATION OF $|V_{us}|$

The data on strange and non-strange spectral moments for the hadronic τ decay provided by ALEPH [26, 63, 64], HFLAV[65], and OPAL [27] collaborations can be used to determine the CKM matrix element $|V_{us}|$. These experimental moments along with the theoretical moments calculated with strange quark mass as input from other sources can be used to determine $|V_{us}|$ using the following relation:

$$|V_{us}| = \sqrt{\frac{R_{\tau,S}^{kl}}{R_{\tau,V+A}^{kl}/|V_{ud}|^2 - \delta R_{\tau,th}^{kl}}}, \quad (62)$$

where $R_{\tau,S}^{kl}$ and $R_{\tau,V+A}^{kl}$ are experimental inputs and $\delta R_{\tau,th}^{kl}$ is the theory input, in which $m_s(2\text{ GeV})$ is taken as an external input. This method has already been used previously in refs. [15, 66–70], and it has been observed that the uncertainties are dominated by the experimental data available for the strange component. An additional source of uncertainties is pointed out in ref. [66] due to s_0 variations which can be cured using a different analysis based on the non-spectral weight functions. However, we have restricted this analysis only to the traditional weight functions.

Using $m_s(2\text{ GeV}) = 93 \pm 11\text{ MeV}$ [32] as an external input and ALEPH data [26, 63, 64], we have presented our determination for $|V_{us}|$ in table VI.

The latest branching fraction of hadronic τ decays into non-strange and slightly more precise strange component from HFLAV[65] can also be used to get more precise determination of $|V_{us}|$ from this method. The results for different schemes are presented in table VII.

The uncertainties shown in these tables are dominated by those coming from the variation of $s_0 \in [2.5, M_\tau^2]$ and

Scheme	$ V_{us} $	
	pQCD inputs	Phenomenological inputs
CIPT	0.2174 ± 0.0045	0.2168 ± 0.0044
FOPT	0.2183 ± 0.0055	0.2179 ± 0.0055
RGSPT	0.2178 ± 0.0046	0.2170 ± 0.0045

TABLE VI: $|V_{us}|$ from ALEPH data in different perturbative scheme using $\delta R_{\tau,th}^{kl}$ from section VII and section VIII.

Scheme	$ V_{us} $	
	pQCD inputs	Phenomenological inputs
CIPT	0.2195 ± 0.0047	0.2189 ± 0.0044
FOPT	0.2205 ± 0.0043	0.2200 ± 0.0037
RGSPT	0.2199 ± 0.0046	0.2191 ± 0.0043

TABLE VII: $|V_{us}|$ from HFLAV data in different perturbative scheme using $\delta R_{\tau,th}^{kl}$ from section VII and section VIII.

experimental uncertainty in strange $R_{\tau,S}$ contributions. It should be noted that uncertainties coming from the variation of the s_0 in table VI and table VII are calculated using the experimental data on the spectral function from ref. [26, 27].

The $|V_{us}|$ determinations from ALEPH [26, 63, 64] and HFLAV[65] are based on $(0,0)$ -moment. A detailed analysis for higher moments can be performed using the OPAL[27] data, where $(k,0)$ moments for $k = 0, \dots, 4$ are also available. These moments are correlated and their correlation should also be considered in the full analysis. Given the large uncertainties in their strange components and unknown precise higher dimensional OPE corrections, we have neglected these correlations

among various moments in our determinations from this data.

Using the strange and non-strange moments from OPAL and the theoretical inputs for $\delta R_{\tau,th}^{kl}$ from Section VII, we present the weighted average of the determination $|V_{us}|$ from prescription I and prescription II in the table VIII. Details of the $|V_{us}|$ from moments along with the sources of uncertainties can be found in table XX and table XXI, respectively. We can observe from these tables that the RGSPT is slightly more sensitive to the strange quark mass taken as input, but the overall theory uncertainty coming in this scheme is lesser than CIPT and FOPT in prescription II. We can also see that the divergent nature of the longitudinal component is still an

issue causing a large theoretical uncertainty dominating in the higher moments in prescription II in the table XXI.

These shortcomings are slightly improved in the phenomenological determination and can be seen in table XXII and table XXIII. Again, these determinations suffer from large s_0 and theoretical uncertainties, especially those coming from the strange quark mass in the higher moments. It is worth emphasizing that prescription I reduces the dependence on the spectral moments in the $|V_{us}|$ determination. The weighted average of these results for $|V_{us}|$ are presented in the table VIII. The RGSPT scheme is slightly more sensitive to the variation of the s_0 , which, compared to CIPT, dominates in the final average presented in the table XXII and can be seen in the table presented in appendix E 3.

Perturbative scheme	$ V_{us} $ from prescription I		$ V_{us} $ from prescription II	
	pQCD inputs	Phenomenological inputs	pQCD inputs	Phenomenological inputs
CIPT	0.2220 ± 0.0050	0.2212 ± 0.0047	0.2232 ± 0.0048	0.2212 ± 0.0045
FOPT	0.2212 ± 0.0059	0.2220 ± 0.0054	0.2240 ± 0.0059	0.2224 ± 0.0054
RGSPT	0.2222 ± 0.0051	0.2215 ± 0.0048	0.2238 ± 0.0049	0.2215 ± 0.0047

TABLE VIII: The weighted average of the determination of $|V_{us}|$ from the OPAL data in the different perturbative schemes.

X. JOINT m_s AND $|V_{us}|$ DETERMINATION

The experimental moments provided by the OPAL collaboration in ref. [27] can be used for the joint extraction of m_s and $|V_{us}|$. It should be noted that the moments provided in the ref. [27] are correlated, and a proper analysis will require their correlations to be taken into account. Given the uncertainties present in the data, we are disregarding these correlations and restrict ourselves to simplified analysis .

Using the phenomenological parametrization for the longitudinal contributions and perturbative “ $L + T$ ”-component from section VI and section IV, we fit the $m_s(2\text{ GeV})$ and $|V_{us}|$ to eq. (62) for moments $(k, 0)$ with $k = 0, 1, \dots, 4$. The central values of the joint fit are presented in table IX. These joint fits give smaller values for $m_s(2\text{ GeV})$ and $|V_{us}|$ compared to the PDG average [32], but very close to the findings of Gamiz et al. [67] for CIPT and RGSPT.

XI. SUMMARY AND CONCLUSION

The hadronic τ decays are important ingredients for extracting various QCD parameters. We have used perturbative schemes CIPT, FOPT, and RGSPT in the extraction of m_s , $|V_{us}|$, and their joint determinations from the experimental inputs available from ALEPH [26, 63, 64], HFLAV[65], and OPAL [27] moments of

Scheme	Phenomenological inputs			
	prescription I		prescription II	
	$m_s(2\text{ MeV})$	$ V_{us} $	$m_s(2\text{ MeV})$	$ V_{us} $
CIPT	75	0.2199	75	0.2199
FOPT	46	0.2227	46	0.2227
RGSPT	73	0.2199	73	0.2199

TABLE IX: Joint determination of $m_s(2\text{ GeV})$ and $|V_{us}|$ from OPAL data with moment $(k, 0)$ with $k=0,1,2,3,4$ in different perturbative scheme from pQCD inputs as well as using phenomenological inputs.

hadronic τ decays. To reach the goal, we first calculate the RGSPT coefficients for the dimension-4 operator and use them for determinations of m_s and $|V_{us}|$. Dimension-6 OPE corrections are known to NLO and their RG-improvement is discussed in ref. [71–73]. Four quark condensates present in these contributions are estimated using the vacuum saturation approximation [74] and found to be numerically very small and are not considered in this article. Higher dimensional OPE corrections are not fully known and are neglected in this article.

The moments calculated using the perturbation theory suffer from convergence issues, so we have employed two prescriptions. The central values of the strange quark mass determinations from prescription I are less spread for different moments than in prescription II. The theoretical uncertainties arising from truncation and scale dependence dominate for higher moments in the prescrip-

tion I for CIPT and FOPT. However, RGSPT has better control over the scale dependence for a wider range of scale variation, even for higher moments as shown in figure 1 and figure 2. This improvement results in a more precise determination in RGSPT compared to FOPT and CIPT schemes.

The important results of this article for the $m_s(M_\tau^2)$ determination are presented in table (IV),(V) and for $|V_{us}|$ determinations in tables (VIII), (VI) and (VII). The joint m_s and $|V_{us}|$ determination results are presented in table IX. It should be noted that the ALEPH moments used in the m_s determinations in this article are based on the old $|V_{us}|$ calculated in ref. [62]. The strange quark mass determinations from the moments are very sensitive to the value of $|V_{us}|$, and hence we do not consider them in the final average. However, the experimental data for the strange and non-strange moments provided by the OPAL collaboration in ref. [27] with the current value of $|V_{us}| = 0.2245 \pm 0.0008$ [32] as an input can be used to provide the most updated determination of the strange quark mass.

We give our final determination for $m_s(M_\tau^2)$, which comes from the weighted average of strange quark mass determination using RGSPT scheme from table V:

$$m_s(M_\tau^2) = 102.0 \pm 19.5 \text{ MeV} \quad (\text{OPAL,RGSPT}), \quad (63)$$

which corresponds to the strange quark mass at 2 GeV :

$$m_s(2 \text{ GeV}) = 98 \pm 19 \text{ MeV} \quad (64)$$

Using ALEPH[26, 64] moment, the $|V_{us}|$ determinations along with their deviation from PDG[32] ($|V_{us}| = 0.2243 \pm 0.0008$) and CKM unitarity fit value ($|V_{us}| = 0.2277 \pm 0.0013$) are:

$$|V_{us}| = 0.2168 \pm 0.0044 \quad (1.7\sigma, 2.6\sigma) \quad (\text{for CIPT}), \quad (65)$$

$$|V_{us}| = 0.2170 \pm 0.0045 \quad (1.6\sigma, 2.3\sigma) \quad (\text{for RGSPT}), \quad (66)$$

and from HFLAV[65]:

$$|V_{us}| = 0.2189 \pm 0.0044 \quad (1.2\sigma, 1.9\sigma) \quad (\text{for CIPT}), \quad (67)$$

$$|V_{us}| = 0.2191 \pm 0.0043 \quad (1.2\sigma, 1.9\sigma) \quad (\text{for RGSPT}). \quad (68)$$

The weighted average of the $|V_{us}|$ determinations from OPAL[27] using phenomenological inputs is presented in table VIII. The most precise determinations for $|V_{us}|$ from this table come from CIPT and RGSPT:

$$|V_{us}| = 0.2212 \pm 0.0047, 0.2212 \pm 0.0045 \quad (\text{for CIPT}), \quad (69)$$

$$|V_{us}| = 0.2215 \pm 0.0048, 0.2215 \pm 0.0047 \quad (\text{for RGSPT}). \quad (70)$$

The mean values of determinations in these schemes are:

$$|V_{us}| = 0.2212 \pm 0.0045 \quad (0.7\sigma, 1.4\sigma) \quad (\text{for CIPT}), \quad (71)$$

$$|V_{us}| = 0.2215 \pm 0.0047 \quad (0.6\sigma, 1.3\sigma) \quad (\text{for RGSPT}). \quad (72)$$

We give our final determinations by weighted average of these results as:

$$|V_{us}| = 0.2189 \pm 0.0044 \quad (1.2\sigma, 1.9\sigma) \quad (\text{for CIPT}), \quad (73)$$

$$|V_{us}| = 0.2191 \pm 0.0043 \quad (1.2\sigma, 1.9\sigma) \quad (\text{for RGSPT}). \quad (74)$$

The values obtained for $|V_{us}|$ using OPAL data agrees with the PDG average within uncertainties. However, the $|V_{us}|$ determination from ALEPH [26, 63, 64] and HFLAV[65] are more than 1.2σ and 1.9σ away from the PDG[32] average and CKM unitarity fit value. It should be noted that the PDG average is already in tension with 2.2σ with the CKM unitarity.

The dependence of our determinations on the choice of the moments and their correlation is not considered in this article, and we expect that these can be further improved using non-spectral weights used by Maltman et al. in ref. [75-77].

XII. ACKNOWLEDGMENTS

We thank Prof. Diogo Boito for providing help with the experimental data on the spectral functions. BA is partly supported by the MSIL Chair of the Division of Physical and Mathematical Sciences, Indian Institute of Science. DD would like to thank the DST, Govt. of India for the INSPIRE Faculty Award (grant no IFA16-PH170). DD also thanks the Institute for Theoretical Physics III, University of Stuttgart for kind hospitality during various stages of the work. AK thanks Shuli Chatterjee, Rhitaja Sengupta, and Prasad Hegde for their valuable discussions. AK is supported by a fellowship from the Ministry of Human Resources Development, Government of India.

Appendix A: Running of the Strong Coupling and the Quark Masses in the pQCD

The running of strong coupling and the quark masses are computed by solving the following differential equations:

$$\mu^2 \frac{d}{d\mu^2} x(\mu^2) = \beta(x(\mu^2)) = - \sum_i x^{i+2}(\mu^2) \beta_i, \quad \mu^2 \frac{d}{d\mu^2} m_i(\mu^2) \equiv m_i(\mu^2) \gamma_m = -m_i(\mu^2) \sum_i \gamma_i x^{i+1}(\mu^2). \quad (\text{A1})$$

The series solutions for the running of strong coupling and the quark masses relevant for contour integration in the complex plane using FOPT are:

$$x(q^2) = x \left\{ 1 + x\beta_0 L + x^2 (\beta_1 L + \beta_0^2 L^2) + x^3 \left(\beta_2 L + \frac{5}{2} \beta_1 \beta_0 L^2 + \beta_0^3 L^3 \right) \right. \\ \left. + x^4 \left(\beta_3 L + \left(\frac{3\beta_1^2}{2} + 3\beta_0 \beta_2 \right) L^2 + \frac{13}{3} \beta_1 \beta_0^2 L^3 + \beta_0^4 L^4 \right) \right. \\ \left. + x^5 \left(\beta_4 L + \left(\frac{7\beta_1 \beta_2}{2} + \frac{7\beta_0 \beta_3}{2} \right) L^2 + (6\beta_2 \beta_0^2 + \frac{35}{6} \beta_1^2 \beta_0) L^3 + \frac{77}{12} \beta_1 \beta_0^3 L^4 + \beta_0^5 L^5 \right) \right\} + \mathcal{O}(\alpha_s^7), \quad (\text{A2})$$

$$m_i(q^2) = m_0 \left\{ 1 + x\gamma_0 L + x^2 \left(\gamma_1 L + \frac{1}{2} \gamma_0 L^2 (\beta_0 + \gamma_0) \right) \right. \\ \left. + x^3 \left(\gamma_2 L + L^2 \left(\frac{\beta_1 \gamma_0}{2} + \gamma_1 (\beta_0 + \gamma_0) \right) + \frac{1}{6} \gamma_0 L^3 (\beta_0 + \gamma_0) (2\beta_0 + \gamma_0) \right) \right. \\ \left. + x^4 \left(\gamma_3 L + L^2 \left(\beta_1 \gamma_1 + \frac{\beta_2 \gamma_0}{2} + \frac{3\beta_0 \gamma_2}{2} + \frac{\gamma_1^2}{2} + \gamma_0 \gamma_2 \right) + \frac{1}{24} \gamma_0 L^4 (\beta_0 + \gamma_0) (2\beta_0 + \gamma_0) (3\beta_0 + \gamma_0) \right. \right. \\ \left. \left. + L^3 \left(\frac{1}{6} (\beta_1 \gamma_0 (5\beta_0 + 3\gamma_0) + 3\gamma_1 (\beta_0 + \gamma_0) (2\beta_0 + \gamma_0)) \right) \right) \right. \\ \left. + x^5 \left(\gamma_4 L + \frac{1}{2} L^2 (\beta_3 \gamma_0 + 3\beta_1 \gamma_2 + 2\gamma_1 (\beta_2 + \gamma_2) + 2\gamma_3 (2\beta_0 + \gamma_0)) \right. \right. \\ \left. \left. + \frac{1}{6} L^3 (3\beta_1^2 \gamma_0 + \beta_1 \gamma_1 (14\beta_0 + 9\gamma_0) + 3(2\beta_0 + \gamma_0) (\beta_2 \gamma_0 + \gamma_2 (2\beta_0 + \gamma_0) + \gamma_1^2)) \right. \right. \\ \left. \left. + \frac{1}{12} L^4 (\beta_1 \gamma_0 (13\beta_0 \gamma_0 + 13\beta_0^2 + 3\gamma_0^2) + 2\gamma_1 (\beta_0 + \gamma_0) (2\beta_0 + \gamma_0) (3\beta_0 + \gamma_0)) \right. \right. \\ \left. \left. + \frac{1}{120} \gamma_0 L^5 (\beta_0 + \gamma_0) (2\beta_0 + \gamma_0) (3\beta_0 + \gamma_0) (4\beta_0 + \gamma_0) \right) \right\} + \mathcal{O}(\alpha_s^6), \quad (\text{A3})$$

where $x \equiv x(\mu^2)$, $L = \log(\mu^2/q^2)$, β_i are the QCD beta function coefficients and γ_i are the coefficients of the anomalous dimension of the quark mass.

The QCD beta function coefficients are known to five-loop [78–86] and their analytic expressions for the active flavor $n_f = 3$ are:

$$\beta_0 = 9/4, \quad \beta_1 = 4, \quad \beta_2 = 3863/384, \quad \beta_3 = 140599/4608 + (445\zeta(3))/32 \\ \beta_4 = \frac{11059213\zeta(3)}{55296} - \frac{534385\zeta(5)}{3072} - \frac{801\pi^4}{2048} + \frac{139857733}{1327104}. \quad (\text{A4})$$

The known five-loop quark mass anomalous dimension coefficients[87–94] for $n_f = 3$ are:

$$\gamma_m^{(0)} = 1, \quad \gamma_m^{(1)} = \frac{91}{24}, \quad \gamma_m^{(2)} = \frac{8885}{576} - \frac{5\zeta(3)}{2}, \quad \gamma_m^{(3)} = -\frac{9295\zeta(3)}{432} - \frac{125\zeta(5)}{12} + \frac{3\pi^4}{32} + \frac{2977517}{41472}, \\ \gamma_m^{(4)} = \frac{156509815}{497664} - \frac{23663747\zeta(3)}{124416} + 85\zeta(3)^2 + \frac{4753\pi^4}{4608} + \frac{118405\zeta(7)}{576} - \frac{22625465\zeta(5)}{62208} + \frac{125\pi^6}{2016}. \quad (\text{A5})$$

We also need the vacuum anomalous dimension for dimension-4 operators, which has been recently computed to

five-loop[95]. Their analytic expression of the diagonal component relevant for this article is given by :

$$\begin{aligned} \hat{\gamma}_0^{di} &\equiv \frac{3}{16\pi^2} \gamma_n^{ii} x^n \\ &= \frac{3}{16\pi^2} \left\{ -1 - \frac{4x}{3} + x^2 \left(\frac{2\zeta(3)}{3} - \frac{223}{72} \right) + x^3 \left(\frac{346\zeta(3)}{9} - \frac{1975\zeta(5)}{54} + \frac{13\pi^4}{540} - \frac{3305}{1296} \right) \right. \\ &\quad \left. + x^4 \left(\frac{6121\zeta(3)^2}{864} - \frac{11881\pi^4}{8640} + \frac{1680599\zeta(3)}{2592} + \frac{36001\zeta(7)}{96} + \frac{93925\pi^6}{326592} - \frac{59711\zeta(5)}{48} + \frac{16141627}{248832} \right) \right\}. \end{aligned} \quad (\text{A6})$$

Appendix B: The RGSP T Coefficients Relevant The Dimension-0 and The Dimension-2 Adler Functions

The first three summed series coefficients are presented as

$$S_0[w] = w^{-n_2 \tilde{\gamma}_0 - n_1} \quad (\text{B1})$$

$$S_1[w] = w^{-n_2 \tilde{\gamma}_0 - n_1 - 1} \left(T_{1,0} - n_1 \tilde{\beta}_1 L_w + n_2 \times (-\tilde{\beta}_1 \tilde{\gamma}_0 + \tilde{\gamma}_1 + w \tilde{\beta}_1 \tilde{\gamma}_0 - \tilde{\beta}_1 \tilde{\gamma}_0 L_w - w \tilde{\gamma}_1) \right) \quad (\text{B2})$$

$$\begin{aligned} S_2[w] &= w^{-n_2 \tilde{\gamma}_0 - n_1 - 2} \left\{ T_{2,0} + T_{1,0} \left(n_2 (\tilde{\gamma}_1 - \tilde{\beta}_1 \tilde{\gamma}_0) + n_2 w (\tilde{\beta}_1 \tilde{\gamma}_0 - \tilde{\gamma}_1) + L_w (-n_2 \tilde{\beta}_1 \tilde{\gamma}_0 - n_1 \tilde{\beta}_1 - \tilde{\beta}_1) \right) \right. \\ &\quad + \left\{ n_1 (\tilde{\beta}_2 - \tilde{\beta}_1^2) + n_2 \left(-\frac{1}{2} \tilde{\beta}_1^2 \tilde{\gamma}_0 - \frac{1}{2} \tilde{\beta}_1 \tilde{\gamma}_1 + \frac{1}{2} \tilde{\beta}_2 \tilde{\gamma}_0 + \frac{\tilde{\gamma}_2}{2} \right) + w \left[n_1 (\tilde{\beta}_1^2 - \tilde{\beta}_2) + n_2 (\tilde{\beta}_1^2 \tilde{\gamma}_0 - \tilde{\beta}_2 \tilde{\gamma}_0) \right] \right. \\ &\quad \left. + n_2^2 \left(-\tilde{\beta}_1 \tilde{\gamma}_0^2 + 2 \tilde{\beta}_1 \tilde{\gamma}_1 \tilde{\gamma}_0 - \tilde{\gamma}_1^2 \right) + L_w \left(n_2^2 (\tilde{\beta}_1 \tilde{\gamma}_0 \tilde{\gamma}_1 - \tilde{\beta}_1^2 \tilde{\gamma}_0^2) + n_1 n_2 (\tilde{\beta}_1 \tilde{\gamma}_1 - \tilde{\beta}_1^2 \tilde{\gamma}_0) \right) \right] \\ &\quad + L_w^2 \left[\frac{1}{2} n_2^2 \tilde{\beta}_1^2 \tilde{\gamma}_0^2 + \frac{1}{2} n_1^2 \tilde{\beta}_1^2 + \frac{1}{2} n_2 \tilde{\beta}_1^2 \tilde{\gamma}_0 + n_1 \left(n_2 \tilde{\beta}_1^2 \tilde{\gamma}_0 + \frac{\tilde{\beta}_1^2}{2} \right) \right] + w^2 \left[n_2^2 \left(\frac{1}{2} \tilde{\beta}_1^2 \tilde{\gamma}_0^2 - \tilde{\beta}_1 \tilde{\gamma}_1 \tilde{\gamma}_0 + \frac{\tilde{\gamma}_1^2}{2} \right) \right. \\ &\quad \left. + n_2 \left(-\frac{1}{2} \tilde{\beta}_1^2 \tilde{\gamma}_0 + \frac{1}{2} \tilde{\beta}_1 \tilde{\gamma}_1 + \frac{1}{2} \tilde{\beta}_2 \tilde{\gamma}_0 - \frac{\tilde{\gamma}_2}{2} \right) \right] \left. \right\} \quad (\text{B3}) \end{aligned}$$

where $\tilde{X}_i \equiv X_i/\beta_0$, and the rest of them can be found by solving eq. (20) with the boundary conditions that $S_i[1] = T_{i,0}$ and for simplification of the expressions, we have taken $T_{0,0} = 1$.

Appendix C: Perturbative coefficients Relevant for the Dimension-4 Corrections and their RGSP T coefficients

The RG-inaccessible coefficients needed for the dimension-4 operators are calculated in ref. [10, 51, 57, 96–103] and their values are:

$$\begin{aligned} p0_0 &= 0, & p0_1 &= 1, & p0_2 &= 7/6, & q0_0 &= 1, & q0_1 &= -1, & q0_2 &= -131/24, & hl0_0 &= 1, & kl0_0 &= 1 \\ t0_0 &= 0, & t0_1 &= 1, & t0_2 &= 17/2, & h0_0 &= 1, & g0_0 &= 1, & g0_1 &= 94/9 - 4/3\zeta_3, & k0_0 &= 0, & k0_1 &= 1. \end{aligned} \quad (\text{C1})$$

Perturbative coefficients involving the condensates terms described in section IV C are:

$$\begin{aligned} p_0^{L+T}(w) &= 0, & p_1^{L+T}(w) &= p0_1, & p_2^{L+T}(w) &= \frac{\beta_1 p0_1}{\beta_0} + \frac{p0_2 - \frac{\beta_1 p0_1}{\beta_0}}{w}, \\ r_0^{L+T}(w) &= 0, & r_1^{L+T}(w) &= \frac{\gamma_0 p0_1}{6\beta_0 w} - \frac{\gamma_0 p0_1}{6\beta_0}, & r_2^{L+T}(w) &= \frac{\frac{\beta_1 \gamma_0 p0_1}{6\beta_0^2} - \frac{\gamma_0 p0_2}{6\beta_0}}{w}, \\ q_0^{L+T}(w) &= q0_0, & q_1^{L+T}(w) &= \frac{q0_1}{w}, & q_2^{L+T}(w) &= \frac{q0_2 - \frac{\beta_1 q0_1 \log(w)}{\beta_0}}{w^2}, \\ t_0^{L+T}(w) &= 0, & t_1^{L+T}(w) &= \frac{t0_1}{w}, & t_2^{L+T}(w) &= \frac{t0_2 - \frac{\beta_1 t0_1 \log(w)}{\beta_0}}{w^2}. \end{aligned} \quad (\text{C2})$$

The RGSPT coefficients for the coefficients of m^4 to $\mathcal{O}(\alpha_s)$ are:

$$k_0^{L+T}(w) = \frac{\gamma_0^{ii} t_0 \left(2(1-w)w^{-\frac{4\gamma_0}{\beta_0}} - 2w^{-\frac{4\gamma_0}{\beta_0}} + 2 \right)}{10w(24\gamma_0 - 2\beta_0)}, \quad g_0^{L+T}(w) = g_0 w^{-\frac{4\gamma_0}{\beta_0}}, \quad j_0^L(w) = 0, \quad j_1^L(w) = 0, \quad (\text{C3})$$

$$k_1^{L+T}(w) = \frac{\gamma_0^{ii} w^{-\frac{4\gamma_0}{\beta_0} - 2}}{10\beta_0(\beta_0 - 4\gamma_0)^2} \left(\beta_1 t_0 \left(w^{\frac{4\gamma_0}{\beta_0}} (\beta_0(\log(w) + 1) - 4\gamma_0 \log(w)) - \beta_0 w \right) - \beta_0 t_0 (\beta_0 - 4\gamma_0) \left(w^{\frac{4\gamma_0}{\beta_0}} - w \right) \right) \\ + k_0 w^{-\frac{4\gamma_0}{\beta_0} - 1} + \frac{\gamma_1^{ii} t_0 - \gamma_1^{ii} t_0 w^{-\frac{4\gamma_0}{\beta_0} - 1}}{104\gamma_0} \quad (\text{C4})$$

$$h_0^{L+T}(w) = h_0 w^{-\frac{4\gamma_0}{\beta_0}} + \frac{q_0 \left(\frac{1}{w} - w^{-\frac{4\gamma_0}{\beta_0}} \right)}{2(\beta_0 - 4\gamma_0)} - \frac{q_0 \gamma_1 w^{-\frac{4\gamma_0}{\beta_0}} \left(\beta_0 \left(w^{\frac{4\gamma_0}{\beta_0}} - 1 \right) - 4\gamma_0 (w - 1) \right)}{2\beta_0 \gamma_0 (\beta_0 - 4\gamma_0)} \\ \frac{q_0 w^{-\frac{4\gamma_0}{\beta_0}} \left(\beta_0^2 (-4\beta_0 + 3\beta_1 + 16\gamma_0) \left(w^{\frac{4\gamma_0}{\beta_0}} - 1 \right) + 12\beta_1 \gamma_0 (4\gamma_0(-w + \log(w) + 1) - \beta_0 \log(w)) \right)}{24\beta_0^2 \gamma_0 (\beta_0 - 4\gamma_0)}, \quad (\text{C5})$$

$$h_1^{L+T}(w) = w^{-\frac{4\gamma_0}{\beta_0} - 1} \left(\frac{h_0 (4\beta_0 \gamma_1 - 4\beta_1 \gamma_0 (\log(w) + 1))}{\beta_0^2} + h_0 + \frac{\beta_1 q_0 \log(w) (3\beta_1 \gamma_0 (\log(w) + 2) - 2\beta_0 (\beta_0 + 3\gamma_1))}{3\beta_0^4} \right) \\ + \frac{q_0 (\beta_0^3 (-4\beta_1 + 16\gamma_1 + 6\gamma_2) + 2\beta_0^2 (3(\beta_2 \gamma_0 + 4\gamma_1^2) - \beta_1 (8\gamma_0 + 9\gamma_1)) + 6\beta_1 \beta_0 \gamma_0 (\beta_1 - 8\gamma_1)) w^{-\frac{4\gamma_0}{\beta_0} - 1}}{6\beta_0^4 (\beta_0 + 4\gamma_0)} \\ + \frac{q_0 (3\beta_2 \gamma_0 + \gamma_1 (4\beta_0 - 3\beta_1 - 16\gamma_0 + 12\gamma_1) - 12\gamma_2 \gamma_0)}{6\gamma_0 (\beta_0^2 - 16\gamma_0^2)} + \frac{\gamma_2^{ii} q_0}{2(\beta_0 - 4\gamma_0)} - \frac{q_0 \left(\gamma_2^{ii} - 8 \frac{\beta_1^2 \gamma_0^2}{\beta_0^4} \right) w^{-\frac{4\gamma_0}{\beta_0} - 1}}{2(\beta_0 + 4\gamma_0)} \\ + \frac{1}{(\beta_0 - 4\gamma_0)} \left\{ \frac{q_0 (\beta_0^3 \gamma_2 - \beta_0^2 (\beta_2 \gamma_0 + \gamma_1 (\beta_1 + 4\gamma_1)) + \beta_1 \beta_0 \gamma_0 (\beta_1 + 8\gamma_1) - 4\beta_1^2 \gamma_0^2) w^{1 - \frac{4\gamma_0}{\beta_0}}}{\beta_0^4} \right. \\ \left. + \frac{q_0 (-4\beta_0 + 3\beta_1 + 16\gamma_0 - 12\gamma_1)}{24\gamma_0} + w^{-\frac{4\gamma_0}{\beta_0}} \left(q_0 \left(\frac{\beta_0}{6\gamma_0} - \frac{\beta_1 - 4\gamma_1}{8\gamma_0} - \frac{2\gamma_1}{\beta_0} + \frac{2\beta_1 \gamma_0 (\log(w) + 1)}{\beta_0^2} - \frac{2}{3} \right) - \frac{q_0}{2} \right) \right. \\ \left. + \frac{\frac{q_0}{2} - \frac{\beta_1 q_0 \log(w)}{2\beta_0}}{w^2} + \frac{2q_0 (\beta_0 \gamma_1 - \beta_1 \gamma_0) w^{-\frac{4\gamma_0}{\beta_0}}}{\beta_0^2} \right\} \quad (\text{C6})$$

$$g_1^{L+T}(w) = -\frac{\beta_1 4\gamma_0 g_0 \log(w) w^{-\frac{4\gamma_0}{\beta_0} - 1}}{\beta_0^2} + \frac{w^{-\frac{4\gamma_0}{\beta_0} - 1} (4\beta_0^2 g_0 + 4\beta_0 \gamma_1 g_0 (1-w) - 4\beta_1 4\gamma_0 g_0 (1-w))}{4\beta_0^2} \quad (\text{C7})$$

$$h_0^L(w) = -\frac{\gamma_0^{ii} w^{-\frac{4\gamma_0}{\beta_0}} \left(\beta_0^2 (\beta_1 - \gamma_1) \left(w^{\frac{4\gamma_0}{\beta_0}} - 1 \right) - \beta_0 4\gamma_0 (\beta_1 \log(w) - \gamma_1 (w - 1)) + \beta_1 4\gamma_0^2 (-w + \log(w) + 1) \right)}{8\beta_0^2 4\gamma_0 (\beta_0 - 4\gamma_0)} \\ + h l_0 w^{-\frac{4\gamma_0}{\beta_0}} + \frac{\gamma_1^{ii} \left(1 - w^{-\frac{4\gamma_0}{\beta_0}} \right)}{84\gamma_0} - \frac{\gamma_0^{ii} (1 - w^{1 - \frac{4\gamma_0}{\beta_0}})}{8x(\beta_0 - 4\gamma_0)}, \quad (\text{C8})$$

$$\begin{aligned}
h_1^L(w) = & w^{-\frac{4\gamma_0}{\beta_0}} \left(-\frac{2\beta_1^2\gamma_0}{\beta_0^4} + \frac{4\beta_1\gamma_1}{\beta_0^3} + \frac{\beta_1\gamma_1}{2\beta_0^2\gamma_0} - \frac{2\gamma_1}{3\beta_0\gamma_0} - \frac{2\gamma_1^2}{\beta_0^2\gamma_0} + \frac{2\beta_1}{3\beta_0^2} - \frac{\beta_2}{2\beta_0^2} + hl_0 \left(\frac{4\beta_1\gamma_0}{\beta_0^2} - \frac{4\gamma_1}{\beta_0} \right) + \frac{\frac{2\gamma_1}{3\gamma_0} + \frac{\gamma_2^{ii}}{2}}{(\beta_0 + 4\gamma_0)} \right. \\
& + \left. \left(\frac{2\beta_1\gamma_1}{\beta_0^3} - \frac{2\beta_1^2\gamma_0}{\beta_0^4} \right) \log(w) \right) + \frac{(\beta_0^3\gamma_2 - \beta_0^2(\beta_2\gamma_0 + \gamma_1(\beta_1 + 4\gamma_1)) + \beta_1\beta_0\gamma_0(\beta_1 + 8\gamma_1) - 4\beta_1^2\gamma_0^2) w^{1-\frac{4\gamma_0}{\beta_0}}}{\beta_0^4(\beta_0 - 4\gamma_0)} \\
& + \frac{-\frac{\gamma_1(\beta_1-4\gamma_1)}{\gamma_0} + \beta_2 - 4\gamma_2}{2(\beta_0^2 - 16\gamma_0^2)} + w^{-\frac{4\gamma_0}{\beta_0}-1} \left\{ hl_0 \left(-\frac{4\beta_1\gamma_0}{\beta_0^2} + \frac{4\gamma_1}{\beta_0} - \frac{4\beta_1\gamma_0 \log(w)}{\beta_0^2} \right) + hl_0 + \frac{\beta_1^2\gamma_0 \log^2(w)}{\beta_0^4} \right. \\
& + \left. \left(\frac{2\beta_1^2\gamma_0}{\beta_0^4} - \frac{2\beta_1\gamma_1}{\beta_0^3} - \frac{2\beta_1}{3\beta_0^2} \right) \log(w) + \frac{1}{6\beta_0^4(\beta_0 + 4\gamma_0)} \left\{ 2\beta_0^2(3(\beta_2\gamma_0 + 4\gamma_1^2) - \beta_1(8\gamma_0 + 9\gamma_1)) \right. \right. \\
& \left. \left. + \beta_0^3(-4\beta_1 + 16\gamma_1 + 6\gamma_2) + 6\beta_1\beta_0\gamma_0(\beta_1 - 8\gamma_1) + 24\beta_1^2\gamma_0^2 - 3\beta_0^4\gamma_2^{ii} \right\} \right\}, \tag{C9}
\end{aligned}$$

$$\begin{aligned}
k_0^L(w) = & -\frac{w^{1-\frac{4\gamma_0}{\beta_0}} - 1}{3(\beta_0 - 4\gamma_0)x} - \frac{1}{9\gamma_0} + \frac{\beta_1 - 4\gamma_1}{12\gamma_0(\beta_0 - 4\gamma_0)} + \frac{4(\beta_0\gamma_1 - \beta_1\gamma_0)w^{1-\frac{4\gamma_0}{\beta_0}}}{3\beta_0^2(\beta_0 - 4\gamma_0)} \\
& + w^{-\frac{4\gamma_0}{\beta_0}} \left(kl_0 + \frac{-3\beta_0(\beta_1 - 4\gamma_1) + 4\beta_0^2 - 12\beta_1\gamma_0(\log(w) + 1)}{36\beta_0^2\gamma_0} \right), \tag{C10}
\end{aligned}$$

$$\begin{aligned}
k_1^L(w) = & kl_0 w^{-\frac{4\gamma_0}{\beta_0}-1} + \frac{2\beta_1 \log(w) w^{-\frac{4\gamma_0}{\beta_0}-1} (2\beta_0\gamma_1 w + \beta_1\gamma_0(\log(w) - 2w))}{3\beta_0^4} + \frac{\gamma_1(4\gamma_1 - \beta_1) + \gamma_0(\beta_2 - 4\gamma_2)}{3\gamma_0(\beta_0^2 - 16\gamma_0^2)} \\
& + \frac{3\gamma_0\gamma_2^{ii} + 4\gamma_1}{9\gamma_0(\beta_0 + 4\gamma_0)} - \frac{4\beta_1 \log(w) (3\beta_0\gamma_1 - 3\beta_1\gamma_0 + \beta_0^2(9\gamma_0 kl_0 + 1)) w^{-\frac{4\gamma_0}{\beta_0}-1}}{9\beta_0^4} + \frac{w^{-\frac{4\gamma_0}{\beta_0}-1}}{9\beta_0^4(\beta_0 + 4\gamma_0)} \left\{ 6\beta_1\beta_0\gamma_0 \right. \\
& \times (\beta_1 - 8\gamma_1) - 2\beta_0^2(\beta_1(9\gamma_1 + 8\gamma_0(9\gamma_0 kl_0 + 1)) - 3(\beta_2\gamma_0 + 4\gamma_1^2)) + \beta_0^4(36\gamma_1 kl_0 - 3\gamma_2^{ii}) + 24\beta_1^2\gamma_0^2 \\
& \left. + 2\beta_0^3(3\gamma_2 - 2(\beta_1 - 4\gamma_1)(9\gamma_0 kl_0 + 1)) \right\} - \frac{4w^{-\frac{4\gamma_0}{\beta_0}-1}}{9\beta_0^4} \beta_1 \log(w) (3\beta_0\gamma_1 - 3\beta_1\gamma_0 + \beta_0^2(9\gamma_0 kl_0 + 1)) \\
& + \frac{2w^{1-\frac{4\gamma_0}{\beta_0}}}{3\beta_0^4(\beta_0 - 4\gamma_0)} (\beta_0^3\gamma_2 - \beta_0^2(\beta_2\gamma_0 + \gamma_1(\beta_1 + 4\gamma_1)) + \beta_1\beta_0\gamma_0(\beta_1 + 8\gamma_1) - 4\beta_1^2\gamma_0^2) + \frac{w^{-\frac{4\gamma_0}{\beta_0}}}{9\beta_0^4\gamma_0} \left\{ 24\beta_1\beta_0\gamma_0\gamma_1 \right. \\
& \left. - 12\beta_1^2\gamma_0^2 - 4\beta_0^3\gamma_1(9\gamma_0 kl_0 + 1) + \beta_0^2(\beta_1(3\gamma_1 + 4\gamma_0(9\gamma_0 kl_0 + 1)) - 3(\beta_2\gamma_0 + 4\gamma_1^2)) \right\} \tag{C11}
\end{aligned}$$

where $w = (1 - \beta_0 xL)$.

Appendix D: Contributions to the Adler Function

1. Dimension-zero contributions

In massless case, Adler function is known to $\mathcal{O}(\alpha_s^4)$ [40–49] and contribution from longitudinal part is zero ($D_{i,j}^{L,(0)} = 0$) while $D_{i,j}^{L+T,0}$ is given by:

$$\begin{aligned}
\mathcal{D}_{i,j}^{L+T,0} = & 1 + x + x^2 \left(\frac{299}{24} - 9\zeta(3) \right) + x^3 \left(-\frac{779\zeta(3)}{4} + \frac{75\zeta(5)}{2} + \frac{58057}{288} \right) \\
& + x^4 \left(\frac{4185\zeta(3)^2}{8} + \frac{729\pi^2\zeta(3)}{16} - \frac{1704247\zeta(3)}{432} + \frac{34165\zeta(5)}{96} - \frac{1995\zeta(7)}{16} - \frac{13365\pi^2}{256} + \frac{78631453}{20736} \right) \tag{D1}
\end{aligned}$$

2. The Dimension-2 Corrections

The dimension-2 correction to the Adler function for the quark flavor i and j is known to $\mathcal{O}(\alpha_s^3)$ [50–55] and the analytic expression reads:

$$\begin{aligned} \mathcal{D}_{2,ij}^{L+T,V/A}(s) = \frac{3}{4\pi^2 s} \left\{ (m_u^2 + m_d^2 + m_s^2) \left(x^2 \left(\frac{8\zeta(3)}{3} - \frac{32}{9} \right) + x^3 \left(4\zeta(3)^2 + \frac{1592\zeta(3)}{27} - \frac{80\zeta(5)}{27} - \frac{2222}{27} \right) \right) \right. \\ + (m_i^2 + m_j^2) \left(1 + \frac{13x}{3} + x^2 \left(\frac{179\zeta(3)}{54} - \frac{520\zeta(5)}{27} + \frac{23077}{432} \right) + x^3 \left(\frac{53\zeta(3)^2}{2} \right. \right. \\ \left. \left. - \frac{1541\zeta(3)}{648} + \frac{79835\zeta(7)}{648} - \frac{54265\zeta(5)}{108} - \frac{\pi^4}{36} + \frac{3909929}{5184} \right) \right) \\ \pm m_i m_j \left(\frac{2x}{3} + x^2 \left(-\frac{55\zeta(3)}{27} - \frac{5\zeta(5)}{27} + \frac{769}{54} \right) + x^3 \left(-\frac{11677\zeta(3)^2}{108} \right. \right. \\ \left. \left. + \frac{70427\zeta(3)}{324} + \frac{82765\zeta(5)}{54} - \frac{555233\zeta(7)}{864} + \frac{\pi^4}{9} - \frac{7429573}{3888} \right) \right) \left. \right\}, \quad (\text{D2}) \end{aligned}$$

where upper and lower signs correspond to vector and axial-vector components, respectively, and this convention is used for the Adler functions in this section. It should be noted that the $\mathcal{O}(\alpha_s^4)$ correction to $m_i m_j$ term has been obtained from eq(15) of ref. [50]. The longitudinal component of the dimension-2 operator is known to $\mathcal{O}(\alpha_s^4)$ [9–14] and has the form:

$$\begin{aligned} \mathcal{D}_{2,ij}^{L,V/A} = \frac{-3}{8\pi^2} \frac{(m_i \mp m_j)^2}{M_\tau^2} \left\{ 1 + \frac{17x}{3} + x^2 \left(\frac{9631}{144} - \frac{35\zeta(3)}{2} \right) + x^3 \left(-\frac{91519\zeta(3)}{216} + \frac{715\zeta(5)}{12} - \frac{\pi^4}{36} + \frac{4748953}{5184} \right) \right. \\ + x^4 \left(\frac{192155\zeta(3)^2}{216} - \frac{46217501\zeta(3)}{5184} + \frac{455725\zeta(5)}{432} - \frac{125\pi^6}{9072} - \frac{52255\zeta(7)}{256} \right. \\ \left. \left. - \frac{3491\pi^4}{10368} + \frac{7055935615}{497664} \right) \right\}. \quad (\text{D3}) \end{aligned}$$

From the above dimension-2 Adler functions, the important piece relevant for Cabibbo suppressed strange quark mass determination [22] using eq. (13) are:

$$\begin{aligned} \delta\mathcal{D}_2^{L+T,V+A}(s) &= (\mathcal{D}_{2,ud}^{L+T,V+A}(s) - \mathcal{D}_{2,us}^{L+T,V+A}(s)) \\ &= \frac{-3m_s^2}{2\pi^2 s} (1 - \epsilon_d^2) \left(1 + \frac{13x}{3} + x^2 \left(\frac{179\zeta(3)}{54} - \frac{520\zeta(5)}{27} + \frac{23077}{432} \right) \right. \\ &\quad \left. + x^3 \left(\frac{53\zeta(3)^2}{2} - \frac{1541\zeta(3)}{648} + \frac{79835\zeta(7)}{648} - \frac{54265\zeta(5)}{108} - \frac{\pi^4}{36} + \frac{3909929}{5184} \right) \right) \quad (\text{D4}) \end{aligned}$$

$$\equiv \frac{-3m_s^2(-\xi^2 s)}{2\pi^2 s} (1 - \epsilon_d^2) \sum_{i=0} \tilde{d}_{i,0}^{L+T}(\xi^2) x(-\xi^2 s)^i \quad (\text{D5})$$

$$= \frac{-3m_s^2(\xi^2 M_\tau^2)}{2\pi^2 s} (1 - \epsilon_d^2) \sum_{i=0}^4 \sum_{j=0}^i \tilde{d}_{i,j}^{L+T} x(\xi^2 M_\tau^2)^i \log^j \left(\frac{\xi^2 M_\tau^2}{-s} \right), \quad (\text{D6})$$

and the corresponding contribution from the longitudinal component is:

$$\begin{aligned} \delta\mathcal{D}_2^{L,V+A}(s) &= \mathcal{D}_{2,ud}^{L,V+A} - \mathcal{D}_{2,us}^{L,V+A} \\ &= \frac{3m_s^2}{4\pi^2 M_\tau^2} (1 - \epsilon_d^2) \left\{ 1 + \frac{17x}{3} + x^2 \left(\frac{9631}{144} - \frac{35\zeta(3)}{2} \right) + x^3 \left(-\frac{91519\zeta(3)}{216} + \frac{715\zeta(5)}{12} - \frac{\pi^4}{36} \right. \right. \\ &\quad \left. \left. + \frac{4748953}{5184} \right) + x^4 \left(\frac{192155\zeta(3)^2}{216} - \frac{46217501\zeta(3)}{5184} + \frac{455725\zeta(5)}{432} - \frac{52255\zeta(7)}{256} \right. \right. \\ &\quad \left. \left. - \frac{125\pi^6}{9072} - \frac{3491\pi^4}{10368} + \frac{7055935615}{497664} \right) \right\} \end{aligned} \quad (D7)$$

$$\equiv \frac{3m_s^2(-\xi^2 s)}{4\pi^2 M_\tau^2} (1 - \epsilon_d^2) \sum_{i=0}^4 \tilde{d}_{i,0}^L(\xi^2) x(-\xi^2 s)^i \quad (D8)$$

$$= \frac{3m_s^2(\xi^2 M_\tau^2)}{4\pi^2 M_\tau^2} (1 - \epsilon_d^2) \sum_{i=0}^4 \sum_{j=0}^i \tilde{d}_{i,j}^L x(\xi^2 M_\tau^2)^i \log^j \left(\frac{\xi^2 M_\tau^2}{-s} \right). \quad (D9)$$

The RGSPT coefficients for the dimension-2 operators can be written in the following form:

$$\begin{aligned} \delta\mathcal{D}_{V+A}^{J,2}(s) &= \text{norm} \times \frac{3m_s^2}{2\pi^2} (1 - \epsilon_d^2) \left\{ \frac{1}{w^{8/9}} + x \left(\frac{\tilde{d}_{1,0}^J}{w^{17/9}} - \frac{1.79012}{w^{8/9}} + \frac{1.79012}{w^{17/9}} - \frac{1.58025 \log(w)}{w^{17/9}} \right) \right. \\ &\quad + x^2 \left(\frac{1.79012 \tilde{d}_{1,0}^J}{w^{26/9}} + \frac{\tilde{d}_{2,0}^J}{w^{26/9}} - \frac{1.79012 \tilde{d}_{1,0}^J}{w^{17/9}} + \frac{(-3.35802 \tilde{d}_{1,0}^J - 8.82061) \log(w)}{w^{26/9}} - \frac{0.339459}{w^{8/9}} \right. \\ &\quad \left. - \frac{4.36949}{w^{17/9}} + \frac{4.70895}{w^{26/9}} + \frac{2.65325 \log^2(w)}{w^{26/9}} + \frac{2.82884 \log(w)}{w^{17/9}} \right) \\ &\quad + x^3 \left(\frac{6.01952 \tilde{d}_{1,0}^J}{w^{35/9}} + \frac{1.79012 \tilde{d}_{2,0}^J}{w^{35/9}} + \frac{\tilde{d}_{3,0}^J}{w^{35/9}} - \frac{0.339459 \tilde{d}_{1,0}^J}{w^{17/9}} - \frac{5.68006 \tilde{d}_{1,0}^J}{w^{26/9}} - \frac{1.79012 \tilde{d}_{2,0}^J}{w^{26/9}} \right. \\ &\quad \left. + \frac{(8.62308 \tilde{d}_{1,0}^J + 27.3673) \log^2(w)}{w^{35/9}} + \frac{(6.01128 \tilde{d}_{1,0}^J + 19.7019) \log(w)}{w^{26/9}} + \frac{0.593473}{w^{8/9}} \right. \\ &\quad \left. - \frac{3.28306}{w^{17/9}} + \frac{(-15.1635 \tilde{d}_{1,0}^J - 5.1358 \tilde{d}_{2,0}^J - 39.8653) \log(w)}{w^{35/9}} - \frac{14.9321}{w^{26/9}} + \frac{17.6217}{w^{35/9}} \right. \\ &\quad \left. - \frac{4.5422 \log^3(w)}{w^{35/9}} - \frac{4.74965 \log^2(w)}{w^{26/9}} + \frac{0.53643 \log(w)}{w^{17/9}} \right) \\ &\quad + x^4 \left(\frac{0.593473 \tilde{d}_{1,0}^J}{w^{17/9}} + \frac{27.6536 \tilde{d}_{1,0}^J}{w^{44/9}} + \frac{7.3301 \tilde{d}_{2,0}^J}{w^{44/9}} + \frac{1.79012 \tilde{d}_{3,0}^J}{w^{44/9}} + \frac{\tilde{d}_{4,0}^J}{w^{44/9}} - \frac{6.29286 \tilde{d}_{1,0}^J}{w^{26/9}} \right. \\ &\quad \left. - \frac{0.339459 \tilde{d}_{2,0}^J}{w^{26/9}} - \frac{21.9542 \tilde{d}_{1,0}^J}{w^{35/9}} - \frac{6.99064 \tilde{d}_{2,0}^J}{w^{35/9}} - \frac{1.79012 \tilde{d}_{3,0}^J}{w^{35/9}} - \frac{12.673}{w^{8/9}} + \frac{11.6487}{w^{17/9}} \right. \\ &\quad \left. + \frac{(1.13991 \tilde{d}_{1,0}^J + 11.9782) \log(w)}{w^{26/9}} + \frac{(-19.8721 \tilde{d}_{1,0}^J - 71.1438) \log^3(w)}{w^{44/9}} - \frac{15.09}{w^{26/9}} \right. \\ &\quad \left. + \frac{(-15.4364 \tilde{d}_{1,0}^J - 59.0364) \log^2(w)}{w^{35/9}} - \frac{60.9336}{w^{35/9}} + \frac{77.0479}{w^{44/9}} + \frac{8.13109 \log^3(w)}{w^{35/9}} \right. \\ &\quad \left. - \frac{(68.5739 \tilde{d}_{1,0}^J + 21.5065 \tilde{d}_{2,0}^J + 6.91358 \tilde{d}_{3,0}^J + 192.701) \log(w)}{w^{44/9}} - \frac{0.937834 \log(w)}{w^{17/9}} \right. \\ &\quad \left. + \frac{(39.8584 \tilde{d}_{1,0}^J + 9.19372 \tilde{d}_{2,0}^J + 111.714) \log(w)}{w^{35/9}} + \frac{7.85071 \log^4(w)}{w^{44/9}} - \frac{0.900672 \log^2(w)}{w^{26/9}} \right. \\ &\quad \left. + \frac{(67.7471 \tilde{d}_{1,0}^J + 17.7534 \tilde{d}_{2,0}^J + 186.459) \log^2(w)}{w^{44/9}} \right) \left. \right\}. \end{aligned} \quad (D10)$$

A more compact form for the above equation is:

$$\delta\mathcal{D}_{V+A}^{J,2}(s) \equiv \text{norm} \times \frac{3m_s^2}{2\pi^2} (1 - \epsilon_d^2) \sum_{i=0}^4 \sum_{k=0}^i \sum_{j=0}^k x^i \tilde{T}_{i,j,k}^J \frac{\log^j(w)}{w^{2\gamma_0/\beta_0+k}}, \quad (\text{D11})$$

where

$$\text{norm} = \begin{cases} \frac{-1}{s}, & \text{if } J = 0 + 1 \\ \frac{1}{2M_\tau^2}, & J = 0, \end{cases} \quad (\text{D12})$$

and \tilde{d}_i^J can be obtained from eq. (D5),(D8).

Appendix E: Details of m_s and $|V_{us}|$ determinations in different schemes and the details of sources of uncertainty

1. Strange quark mass determinations using pQCD inputs

In this section, the strange quark mass is calculated using the longitudinal component calculated using OPE as described in sec. V. As mentioned before, these contributions are poorly convergent, and the strange quark mass determinations will suffer from the large truncation uncertainties in addition to significant dependence on the moments used. The dependence on the moment can be slightly reduced by using the prescription I at the cost of enhanced truncation uncertainty. This behavior in the different perturbative schemes and the details of various sources of uncertainties are discussed in the later subsections.

a. Strange quark mass determination using CIPT scheme

Determination of $m_s(M_\tau^2)$ using CIPT are based on dimension-2 contributions described in section[V A]. Using prescription-I, can see that dimension-2 contributions are truncated at $\mathcal{O}(\alpha_s^3)$, $\mathcal{O}(\alpha_s^3)$, $\mathcal{O}(\alpha_s^2)$ and $\mathcal{O}(\alpha_s)$ for $k = 0, 1, 2, 3$ and 4 respectively. This truncation result into the enhancement in the total uncertainty in the $m_s(M_\tau^2)$ determination and can be seen in the tables[X,XI]. However, the main advantage of using prescription-I is that the masses from various moments, using different experimental inputs, agree within the uncertainty, which is not the case in using prescription-2. For this reason, we are presenting $m_s(M_\tau^2)$ from both prescriptions for different schemes in other schemes too.

Parameter	Moments ALEPH[62]					Moment OPAL[27]				
	(0,0)	(1,0)	(2,0)	(3,0)	(4,0)	(0,0)	(1,0)	(2,0)	(3,0)	(4,0)
$m_s(M_\tau^2)$	135 ⁺³⁴ ₋₃₇	122 ⁺²⁸ ₋₂₄	120 ⁺³² ₋₂₄	105 ⁺³¹ ₋₂₃	108 ⁺³⁸ ₋₂₄	124 ⁺³⁰ ₋₃₁	106 ⁺²⁷ ₋₂₆	105 ⁺³⁰ ₋₂₅	94 ⁺²⁹ ₋₂₂	100 ⁺³⁶ ₋₂₄
$\delta R_\tau^{kl}(\text{Exp.})$	+27.4 -34.8	+15.4 -17.7	+11.7 -13.0	+9.4 -10.4	+9.0 -9.9	+23.2 -28.7	+17.8 -21.6	+14.4 -16.8	+11.2 -12.8	+10.6 -12.0
$\xi \in [.75, 2.0]$	+14.3 -6.2	+17.3 -8.0	+20.8 -10.4	+21.1 -10.9	+23.8 -13.4	+13.4 -5.8	+15.1 -7.1	+18.5 -9.2	+19.0 -9.9	+22.1 -12.5
Truncation uncertainty	-8.7 +10.7	-9.4 +12.2	-12.1 +17.3	-11.4 +16.8	-15.6 +26.7	-8.0 +10.0	-8.2 +10.6	-10.7 +15.3	-10.3 +15.2	-14.5 +25.1
$s_0 \in [3, M_\tau^2] (\text{GeV}^2)$	8.3	11.1	12.7	12.5	6.4	7.7	9.6	11.2	11.2	5.9

TABLE X: Strange quark mass using CIPT in prescription I. Other sources of uncertainties are not shown in the table, but are added in the quadrature for $m_s(M_\tau^2)$ in the second row.

Parameter	Moments ALEPH[62]					Moment OPAL[27]				
	(0,0)	(1,0)	(2,0)	(3,0)	(4,0)	(0,0)	(1,0)	(2,0)	(3,0)	(4,0)
$m_s(M_\tau^2)$	126 ⁺³¹ ₋₃₅	112 ⁺²⁶ ₋₂₂	96 ⁺²⁵ ₋₁₉	82 ⁺²⁵ ₋₁₈	69 ⁺²⁴ ₋₁₇	116 ⁺²⁷ ₋₂₉	97 ⁺²⁵ ₋₂₄	84 ⁺²⁴ ₋₂₀	73 ⁺²³ ₋₁₈	64 ⁺²³ ₋₁₆
$\delta R_\tau^{kl}(\text{Exp.})$	+25.7 -32.6	+14.1 -16.3	+9.5 -10.5	+7.4 -8.1	+5.9 -6.4	+21.7 -26.9	+16.4 -19.8	+11.6 -13.6	+8.8 -10.0	+6.9 -7.8
$\xi \in [.75, 2.0]$	+13.2 -6.4	+16.3 -8.3	+18.0 -9.4	+18.7 -10.0	+18.6 -10.1	+12.3 -6.0	+14.3 -7.2	+15.9 -8.3	+16.8 -9.0	+17.1 -9.3
Truncation uncertainty	-7.3 +8.8	-8.0 +10.1	-8.0 +10.6	-7.7 +10.6	-7.2 +10.4	-6.7 +8.1	-6.9 +8.8	-7.0 +9.3	-6.9 +9.6	-6.6 +9.6
$s_0 \in [3, M_\tau^2] (\text{GeV}^2)$	7.8	10.2	10.2	9.7	9.1	7.2	8.8	9.0	8.7	8.5

TABLE XI: CIPT determination of strange quark mass using in prescription II. Only significant sources of uncertainty are shown in the table separately, while the rest are added in the quadrature and appear in $m_s(M_\tau^2)$.

b. Strange quark mass determination using FOPT scheme

The effect of different prescription used is very significant in the FOPT where perturbative contributions from dimension-2 Alder function are truncated at $\mathcal{O}(\alpha_s^4)$ and $\mathcal{O}(\alpha_s^2)$ for for the moment $k = 0$ and 1 while rest of them are truncated at $\mathcal{O}(\alpha_s)$. The final results for $m_s(M_\tau^2)$ determination using FOPT in prescriptions I and II are presented in tables XII and XIII, respectively.

Parameter	Moments ALEPH[62]					Moment OPAL[27]				
	(0,0)	(1,0)	(2,0)	(3,0)	(4,0)	(0,0)	(1,0)	(2,0)	(3,0)	(4,0)
$m_s(M_\tau^2)$	114^{+33}_{-34}	134^{+38}_{-30}	147^{+48}_{-34}	137^{+45}_{-31}	127^{+29}_{-29}	106^{+29}_{-29}	116^{+35}_{-31}	130^{+45}_{-33}	124^{+43}_{-30}	118^{+40}_{-29}
$\delta R_\tau^{kl}(\text{Exp.})$	+23.2 -29.3	+16.5 -19.0	+13.7 -15.4	+11.5 -12.8	+9.9 -11.0	+19.6 -24.2	+19.1 -23.2	+17.0 -19.9	+13.9 -16.0	+11.8 -13.5
$\xi \in [.75, 2.0]$	+19.0 -11.0	+22.6 -12.8	+23.7 -13.5	+21.7 -12.3	+19.5 -11.1	+17.6 -10.2	+19.8 -11.2	+21.2 -12.0	+19.7 -11.1	+18.0 -10.2
Truncation uncertainty	-8.0 +10.1	-14.7 +21.7	-21.5 +36.7	-20.2 +34.5	-18.9 +32.2	-7.4 +9.3	-12.8 +19.0	-19.2 +33.3	-18.5 +32.1	-17.8 +30.7
$s_0 \in [3, M_\tau^2] (\text{GeV}^2)$	8.7	13.2	15.7	15.3	15.4	8.0	11.5	13.9	13.8	14.3

TABLE XII: Strange quark mass using FOPT in prescription I. Other sources of uncertainties are not shown in the table but are added in the quadrature and appear for $m_s(M_\tau^2)$ in the second row.

Parameter	Moments ALEPH[62]					Moment OPAL[27]				
	(0,0)	(1,0)	(2,0)	(3,0)	(4,0)	(0,0)	(1,0)	(2,0)	(3,0)	(4,0)
$m_s(M_\tau^2)$	114^{+33}_{-34}	107^{+30}_{-24}	97^{+28}_{-20}	87^{+27}_{-20}	78^{+25}_{-19}	106^{+29}_{-29}	93^{+28}_{-25}	85^{+26}_{-21}	78^{+25}_{-19}	72^{+24}_{-18}
$\delta R_\tau^{kl}(\text{Exp.})$	+23.2 -29.3	+13.3 -15.2	+9.3 -10.4	+7.6 -8.4	+6.5 -7.1	+19.6 -24.2	+15.3 -18.5	+11.4 -13.3	+9.1 -10.4	+7.6 -8.6
$\xi \in [.75, 2.0]$	+19.0 -11.0	+20.8 -12.2	+20.8 -12.2	+19.8 -11.7	+18.4 -10.8	+17.6 -10.2	+18.1 -10.6	+18.2 -10.7	+17.7 -10.4	+16.9 -9.9
Truncation uncertainty	-8.0 +10.1	-9.0 +12.0	-9.1 +12.7	-8.9 +12.8	-8.5 +12.5	-7.4 +9.3	-7.8 +10.5	-8.1 +11.2	-8.0 +11.5	-7.8 +11.6
$s_0 \in [3, M_\tau^2] (\text{GeV}^2)$	8.7	10.5	10.6	10.3	10.1	8.0	9.1	9.3	9.3	9.4

TABLE XIII: Strange quark mass using FOPT in prescription II. Other sources of uncertainties are not shown in the table but are added in the quadrature and appear for $m_s(M_\tau^2)$ in the second row

c. Strange quark mass determination using the RGSPT scheme

The RGSPT determination of strange quark mass is presented in tables (XIV),(XV) and the most crucial feature of this scheme is that it provides minimum scale uncertainty compared to the CIPT and FOPT. Another important advantage we can infer from prescription II is that it gives the lowest uncertainty among other perturbative schemes.

Parameter	Moments ALEPH[62]					Moment OPAL[27]				
	(0,0)	(1,0)	(2,0)	(3,0)	(4,0)	(0,0)	(1,0)	(2,0)	(3,0)	(4,0)
$m_s(M_\tau^2)$	123^{+28}_{-34}	121^{+23}_{-23}	120^{+26}_{-23}	125^{+37}_{-27}	113^{+35}_{-25}	114^{+24}_{-28}	104^{+23}_{-25}	105^{+25}_{-24}	113^{+35}_{-27}	104^{+33}_{-25}
$\delta R_\tau^{kl}(\text{Exp.})$	+25.2 -32.0	+15.2 -17.4	+11.6 -13.0	+10.9 -12.0	+9.1 -10.1	+21.3 -26.3	+17.5 -21.2	+14.3 -16.7	+13.1 -15.0	+10.8 -12.3
$\xi \in [.75, 2]$	+3.3 -2.1	+4.3 -2.8	+5.1 -3.4	+6.2 -4.2	+5.9 -4.0	+3.0 -2.0	+3.7 -2.4	+4.6 -3.0	+5.7 -3.8	+5.5 -3.7
Truncation uncertainty	-7.2 +8.7	-9.7 +12.8	-12.7 +18.5	-18.2 +31.3	-16.9 +29.6	-6.7 +8.1	-8.4 +11.1	-11.2 +16.4	-16.5 +28.8	-15.8 +27.9
$s_0 \in [3, M_\tau^2] (\text{GeV}^2)$	8.1	11.4	13.1	15.1	14.6	7.5	9.9	11.5	13.6	13.5

TABLE XIV: Strange quark mass using RGSPT in prescription I. Other sources of uncertainties are not shown in the table but are added in the quadrature and appear for $m_s(M_\tau^2)$ in the second row.

Parameter	Moments ALEPH[62]					Moment OPAL[27]				
	(0,0)	(1,0)	(2,0)	(3,0)	(4,0)	(0,0)	(1,0)	(2,0)	(3,0)	(4,0)
$m_s(M_\tau^2)$	123^{+28}_{-34}	110^{+21}_{-21}	95^{+18}_{-17}	82^{+17}_{-16}	70^{+16}_{-14}	114^{+24}_{-28}	95^{+21}_{-23}	84^{+18}_{-18}	74^{+17}_{-16}	65^{+16}_{-14}
$\delta R_\tau^{kl}(\text{Exp.})$	+25.2 -32.0	+13.9 -16.0	+9.4 -10.4	+7.3 -8.1	+5.9 -6.5	+21.3 -26.3	+16.1 -19.4	+11.5 -13.4	+8.8 -10.0	+7.0 -7.9
$\xi \in [.75, 2.0]$	+3.3 -2.1	+4.0 -2.6	+4.3 -2.8	+4.4 -2.9	+4.4 -2.9	+3.0 -2.0	+3.4 -2.3	+3.8 -2.5	+4.0 -2.6	+4.1 -2.7
Truncation uncertainty	-7.2 +8.7	-8.1 +10.3	-8.2 +10.9	-7.9 +11.1	-7.5 +10.9	-6.7 +8.1	-7.0 +8.9	-7.2 +9.6	-7.1 +10.0	-6.9 +10.1
$s_0 \in [3, M_\tau^2] (\text{GeV}^2)$	8.1	10.4	10.4	9.9	9.3	7.5	9.0	9.1	8.9	8.6

TABLE XV: RGSPT determination of strange quark mass using in prescription II. Only the main sources of uncertainty are shown separately, while the rest are added directly in the quadrature of $m_s(M_\tau^2)$.

2. The strange quark mass determinations using phenomenological inputs

In this section, the strange quark mass is calculated using the phenomenological parametrization along with the perturbative “ $L + T$ ”-contributions described in section VI and section IV. The quark mass is calculated in the two prescriptions for various moments, and the details of sources of uncertainties are presented in the tables.

a. Strange quark mass determination using CIPT scheme

The CIPT determination of $m_s(M_\tau^2)$ in this section makes use of the full dimension-2 results of $\mathcal{O}(\alpha_s^3)$ as the series presented in eq. (41) is convergent for all moments, and prescription I and prescription II yield the same determinations. The results are shown in the table XVI.

Parameter	Moments ALEPH[62]						Moment OPAL[27]					
	(0,0)	(1,0)	(2,0)	(3,0)	(4,0)	(4,0) ⁰	(0,0)	(1,1)	(2,0)	(3,0)	(4,0)	(4,0) ⁰
$m_s(M_\tau^2)$	187^{+63}_{-81}	162^{+31}_{-34}	136^{+25}_{-24}	115^{+25}_{-20}	98^{+22}_{-15}	98^{+25}_{-19}	166^{+54}_{-69}	134^{+34}_{-41}	116^{+26}_{-27}	102^{+24}_{-21}	91^{+21}_{-16}	91^{+24}_{-19}
$\delta R_\tau^{kl}(\text{Exp.})$	+57.2 -79.0	+25.5 -30.1	+15.5 -17.5	+11.4 -12.7	+8.8 -9.7	+8.8 -9.7	+49.0 -67.8	+30.2 -39.0	+19.4 -23.3	+13.8 -16.0	+10.5 -11.9	+10.5 -11.9
$\xi \in [.75, 2.0]$	-9.5 +22.9	-1.0 +9.1	+10.8 -0.1	+14.4 -1.7	+16.3 -3.8	+16.3 -3.8	-7.9 +19.5	-0.7 +7.1	+9.5 -0.2	+12.8 -1.6	+14.8 -3.5	+14.8 -3.5
Truncation uncertainty	+3.3 -3.1	+4.5 +4.9	-7.1 +8.4	-7.9 +10.0	-8.1 +10.8	+2.8 -2.7	+2.8 -2.7	-3.7 +4.0	-6.0 +7.1	-7.0 +8.9	-7.5 +9.9	-7.5 +9.9
$s_0 \in [3, M_\tau^2] (\text{GeV}^2)$	11.6	14.7	14.5	13.7	5.8	13.0	10.2	12.9	12.8	12.2	5.2	11.7

TABLE XVI: Strange quark mass using CIPT using phenomenological inputs for the longitudinal component. Only the main sources of uncertainty are shown separately, while the rest are already added to the quadrature and appear in the total uncertainty in $m_s(M_\tau^2)$.

b. Strange quark mass determination using FOPT scheme

The FOPT determination of $m_s(M_\tau^2)$ in this section involves determination in both prescription (I-II) as the perturbation series is not well convergent for different moments, as shown in eq. (47). The results are presented in table XVII and table XVIII.

Parameter	Moments ALEPH[62]					Moment OPAL[27]				
	(0,0)	(1,0)	(2,0)	(3,0)	(4,0)	(0,0)	(1,0)	(2,0)	(3,0)	(4,0)
$m_s(M_\tau^2)$	141^{+46}_{-60}	133^{+35}_{-31}	135^{+38}_{-29}	145^{+50}_{-33}	135^{+46}_{-31}	125^{+40}_{-51}	111^{+34}_{-35}	116^{+36}_{-30}	130^{+46}_{-33}	125^{+44}_{-30}
$\delta R_\tau^{kl}(M_\tau^2)(\text{Exp.})$	+41.2 -57.9	+20.5 -24.2	+15.0 -16.9	+13.8 -15.4	+11.4 -12.7	+35.6 -49.8	+24.3 -31.2	+18.7 -22.5	+16.7 -19.5	+13.6 -15.6
$\xi \in [.75, 2]$	+16.5 -6.4	+21.7 -10.5	+24.5 -12.0	+25.5 -12.6	+23.0 -11.4	+14.8 -5.8	+18.1 -8.8	+21.0 -10.3	+22.7 -11.2	+21.1 -10.4
Truncation uncertainty	-5.8 +6.7	-9.7 +12.4	-14.4 +21.1	-21.2 +36.8	-19.9 +34.4	-5.1 +5.9	-8.0 +10.2	-12.4 +18.2	-19.0 +33.4	-18.6 +32.4
$s_0 \in [3, M_\tau^2] (\text{GeV}^2)$	10.7	13.1	14.4	16.2	16.3	9.5	11.6	12.8	14.6	14.9

TABLE XVII: FOPT determination of $m_s(M_\tau^2)$ using prescription I. Only major sources of uncertainty are shown separately, while the rest are added to the quadrature and appear in the total uncertainty in $m_s(M_\tau^2)$.

Parameter	Moments ALEPH[62]					Moment OPAL[27]				
	(0,0)	(1,0)	(2,0)	(3,0)	(4,0)	(0,0)	(1,0)	(2,0)	(3,0)	(4,0)
$m_s(M_\tau^2)$	141^{+46}_{-60}	133^{+35}_{-31}	121^{+26}_{-33}	109^{+32}_{-23}	99^{+30}_{-22}	125^{+40}_{-51}	111^{+34}_{-35}	104^{+31}_{-27}	97^{+29}_{-23}	91^{+28}_{-22}
$\delta R_\tau^{kl}(M_\tau^2)$ (Exp.)	+41.2 -57.9	+20.5 -24.2	+15.0 -16.9	+13.8 -15.4	+11.4 -12.7	+35.6 -49.8	+24.3 -31.2	+18.7 -22.5	+16.7 -19.5	+13.6 -15.6
$\xi \in [.75, 2]$	$8^{+16.5}_{-6.4}$	+21.7 -10.5	+24.5 -12.0	+25.5 -12.6	+23.0 -11.4	+14.8 -5.8	+18.1 -8.8	+21.0 -10.3	+22.7 -11.2	+21.1 -10.4
Truncation uncertainty	-5.8 +6.7	-9.7 +12.4	-10.4 +14.5	-10.7 +15.1	-10.4 +15.2	-5.1 +5.9	-8.0 +10.2	-9.2 +12.5	-9.6 +13.5	-9.7 +14.1
$s_0 \in [3, M_\tau^2]$ (GeV ²)	10.7	13.1	13.3	13.0	12.8	9.5	11.6	11.7	11.6	11.7

TABLE XVIII: The FOPT determination of $m_s(M_\tau^2)$ in prescription II. Only major sources of uncertainty are shown separately, while the rest are added to the quadrature and appear in the total uncertainty in $m_s(M_\tau^2)$.

c. Strange quark mass determination using RGSPt scheme

The RGSPt determination in prescriptions I-II is shown in the table XIX as the (4,0)-moment is not term by term convergent till $\mathcal{O}(\alpha_s^3)$.

Parameter	Moments ALEPH[62]						Moment OPAL[27]					
	(0,0)	(1,0)	(2,0)	(3,0)	(4,0)	(4,0) ⁰	(0,0)	(1,0)	(2,0)	(3,0)	(4,0)	(4,0) ⁰
$m_s(M_\tau^2)$ (in MeV)	178^{+57}_{-77}	154^{+29}_{-33}	130^{+23}_{-23}	111^{+21}_{-20}	108^{+25}_{-21}	96^{+20}_{-18}	157^{+49}_{-66}	127^{+32}_{-39}	112^{+24}_{-26}	99^{+21}_{-21}	100^{+24}_{-21}	89^{+19}_{-18}
δR_τ^{kl} (Exp.)	+55.8 -75.5	+24.5 -28.7	+14.9 -16.8	+11.0 -12.2	+9.6 -10.6	+8.6 -9.4	+47.4 -64.6	+28.8 -37.0	+18.5 -22.3	+13.3 -15.4	+11.4 -12.9	+10.1 -11.5
$\xi \in [.75, 2]$	-2.7 +2.6	+1.1 -0.2	+2.9 -1.5	-3.7 -2.1	+4.6 -2.7	+4.0 -2.3	-2.2 +2.1	+1.1 -0.3	-2.5 -1.4	+3.3 -1.9	+4.3 -2.5	+3.7 -2.2
Truncation uncertainty	+2.9 -2.7	-5.4 +6.1	-7.9 +9.7	-8.7 +11.3	-11.6 +16.9	-8.8 +12.1	+2.5 -2.4	-4.4 +4.9	-6.8 +8.3	-7.7 +10.1	-10.7 +15.6	-8.1 +11.1
$s_0 \in [3, M_\tau^2]$ (GeV ²)	11.7	14.5	14.2	13.4	12.8	10.3	12.8	12.5	12.5	12.0	12.8	11.6

TABLE XIX: Strange quark mass using RGSPt. Other sources of uncertainties are not shown in the table but are added in the quadrature and appear for $m_s(M_\tau^2)$ in the second row.

3. Details of the $|V_{us}|$ determinations from OPAL data

The CKM matrix element $|V_{us}|$ is calculated using eq. (62) from the available data on moments for strange and non-strange components. Details of extraction from these moments and associated uncertainties from the inputs parameters are presented in this section. Purely pQCD inputs for the longitudinal component is used to extract $|V_{us}|$ in the table XX and table XXI. Large theoretical uncertainties in prescription II come from the truncation of perturbative series. Determination of $|V_{us}|$ from the phenomenological inputs for longitudinal contribution is presented in the table XXII and table XXIII for prescriptions I and II, respectively.

Parameters	$ V_{us} _{CIPT}$					$ V_{us} _{FOPT}$					$ V_{us} _{RGSPt}$					
	(0,0)	(1,0)	(2,0)	(3,0)	(4,0)	(0,0)	(1,0)	(2,0)	(3,0)	(4,0)	(0,0)	(1,0)	(2,0)	(3,0)	(4,0)	
$ V_{us} $ (central)	0.2217	0.2224	0.2219	0.2241	0.2220	0.2227	0.2208	0.2183	0.2181	0.2182	0.2221	0.2229	0.2223	0.2204	0.2217	
m_s	+0.0014 -0.0012	+0.0021 -0.0018	+0.0025 -0.0022	+0.0038 -0.0031	+0.0037 -0.0031	+0.0017 -0.0015	+0.0017 -0.0014	+0.0016 -0.0014	+0.0021 -0.0018	+0.0027 -0.0022	+0.0015 -0.0013	+0.0022 -0.0019	+0.0027 -0.0023	+0.0027 -0.0023	+0.0037 -0.0031	
Experimental	+0.0033 -0.0034	+0.0037 -0.0037	+0.0036 -0.0037	+0.0037 -0.0038	+0.0038 -0.0038	+0.0033 -0.0034	+0.0036 -0.0037	+0.0036 -0.0036	+0.0036 -0.0037	+0.0037 -0.0038	+0.0033 -0.0034	+0.0037 -0.0037	+0.0037 -0.0037	+0.0037 -0.0037	+0.0038 -0.0038	
Total theory	+0.0017 -0.0017	+0.0028 -0.0029	+0.0040 -0.0042	+0.0065 -0.0065	+0.0078 -0.0074	+0.0024 -0.0024	+0.0027 -0.0028	+0.0032 -0.0032	+0.0032 -0.0041	+0.0042 -0.0051	+0.0053 -0.0015	+0.0017 -0.0026	+0.0028 -0.0026	+0.0039 -0.0036	+0.0050 -0.0047	+0.0070 -0.0064
$s_0 \in [2.50, M_\tau^2]$	0.0032	0.0070	0.0117	0.0188	0.0229	0.0042	0.0089	0.0122	0.0146	0.0200	0.0034	0.0074	0.0126	0.0204	0.0272	
total	+0.0049 -0.0050	+0.0084 -0.0085	+0.0129 -0.0129	+0.0203 -0.0203	+0.0245 -0.0244	+0.0058 -0.0059	+0.0100 -0.0100	+0.0131 -0.0131	+0.0156 -0.0156	+0.0210 -0.0210	+0.0051 -0.0050	+0.0088 -0.0087	+0.0137 -0.0136	+0.0213 -0.0213	+0.0283 -0.0282	

TABLE XX: Determination of $|V_{us}|$ in various schemes from the OPAL data using prescription I. The longitudinal component is calculated using the pQCD Adler function.

⁰ prescription II is used for these moments.

Parameters	$ V_{us} _{CIPT}$					$ V_{us} _{FOPT}$					$ V_{us} _{RGSPt}$				
	(0,0)	(1,0)	(2,0)	(3,0)	(4,0)	(0,0)	(1,0)	(2,0)	(3,0)	(4,0)	(0,0)	(1,0)	(2,0)	(3,0)	(4,0)
$ V_{us} $ (central)	0.2217	0.2239	0.2275	0.2341	0.2452	0.2227	0.2246	0.2271	0.2310	0.2365	0.2221	0.2246	0.2286	0.2358	0.2477
m_s	+0.0014 -0.0012	+0.0025 -0.0021	+0.0043 -0.0036	+0.0072 -0.0059	+0.0126 -0.0097	+0.0017 -0.0015	+0.0028 -0.0024	+0.0042 -0.0035	+0.0062 -0.0051	+0.0090 -0.0072	+0.0015 -0.0013	+0.0027 -0.0023	+0.0047 -0.0039	+0.0079 -0.0064	+0.0138 -0.0105
Experimental	+0.0033 -0.0034	+0.0037 -0.0038	+0.0037 -0.0038	+0.0039 -0.0040	+0.0042 -0.0043	+0.0033 -0.0034	+0.0037 -0.0038	+0.0037 -0.0038	+0.0039 -0.0039	+0.0041 -0.0041	+0.0033 -0.0034	+0.0037 -0.0038	+0.0038 -0.0038	+0.0039 -0.0040	+0.0043 -0.0043
Total theory	+0.0017 -0.0017	+0.0033 -0.0035	+0.0063 -0.0065	+0.0121 -0.0116	+0.0237 -0.0206	+0.0024 -0.0024	+0.0043 -0.0043	+0.0071 -0.0068	+0.0110 -0.0102	+0.0165 -0.0147	+0.0017 -0.0015	+0.0033 -0.0030	+0.0061 -0.0055	+0.0109 -0.0096	+0.0200 -0.0168
$s_0 \in [2.5, M_\tau^2]$	0.0030	0.0070	0.0117	0.0188	0.0313	0.0042	0.0089	0.0143	0.0216	0.0325	0.0032	0.0074	0.0126	0.0204	0.0338
total	+0.0048 -0.0048	+0.0086 -0.0087	+0.0138 -0.0139	+0.0227 -0.0225	+0.0395 -0.0377	+0.0058 -0.0059	+0.0106 -0.0162	+0.0164 -0.0163	+0.0245 -0.0242	+0.0368 -0.0359	+0.0049 -0.0049	+0.0089 -0.0089	+0.0145 -0.0145	+0.0235 -0.0229	+0.0395 -0.0380

TABLE XXI: Determination of $|V_{us}|$ in different schemes from the OPAL data using prescription II. The longitudinal component is calculated using the pQCD Adler function.

Parameters	$ V_{us} _{CIPT}$					$ V_{us} _{FOPT}$					$ V_{us} _{RGSPt}$				
	(0,0)	(1,0)	(2,0)	(3,0)	(4,0)	(0,0)	(1,0)	(2,0)	(3,0)	(4,0)	(0,0)	(1,0)	(2,0)	(3,0)	(4,0)
$ V_{us} $ (central)	0.2211	0.2210	0.2212	0.2228	0.2226	0.2222	0.2224	0.2225	0.2208	0.2177	0.2213	0.2213	0.2219	0.2238	0.2233
m_s	+0.0005 -0.0004	+0.0010 -0.0009	+0.0018 -0.0015	+0.0029 -0.0025	+0.0036 -0.0030	+0.0008 -0.0007	+0.0014 -0.0012	+0.0022 -0.0019	+0.0024 -0.0021	+0.0022 -0.0019	+0.0005 -0.0004	+0.0011 -0.0009	+0.0019 -0.0017	+0.0032 -0.0028	+0.0038 -0.0032
Experimental	+0.0033 -0.0034	+0.0036 -0.0037	+0.0036 -0.0037	+0.0037 -0.0038	+0.0038 -0.0038	+0.0033 -0.0034	+0.0037 -0.0037	+0.0037 -0.0037	+0.0037 -0.0037	+0.0037 -0.0038	+0.0033 -0.0034	+0.0036 -0.0037	+0.0036 -0.0037	+0.0037 -0.0038	+0.0038 -0.0039
Total theory	+0.0005 -0.0005	+0.0010 -0.0010	+0.0020 -0.0020	+0.0036 -0.0037	+0.0062 -0.0054	+0.0009 -0.0009	+0.0019 -0.0019	+0.0033 -0.0033	+0.0039 -0.0039	+0.0043 -0.0041	+0.0005 -0.0004	+0.0011 -0.0010	+0.0022 -0.0020	+0.0040 -0.0036	+0.0055 -0.0050
$s_0 \in [2.5, M_\tau^2]$	0.0032	0.0070	0.0117	0.0188	0.0229	0.0042	0.0089	0.0122	0.0146	0.0200	0.0034	0.0074	0.0126	0.0204	0.0272
total	+0.0047 -0.0047	+0.0080 -0.0080	+0.0124 -0.0124	+0.0195 -0.0195	+0.0238 -0.0239	+0.0054 -0.0054	+0.0098 -0.0099	+0.0131 -0.0132	+0.0155 -0.0155	+0.0208 -0.0207	+0.0048 -0.0048	+0.0084 -0.0084	+0.0133 -0.0133	+0.0211 -0.0211	+0.0280 -0.0279

TABLE XXII: Determination of $|V_{us}|$ in different schemes from the OPAL data using prescription I. The phenomenological contributions are used for longitudinal components.

Parameters	$ V_{us} _{CIPT}$					$ V_{us} _{FOPT}$					$ V_{us} _{RGSPt}$				
	(0,0)	(1,0)	(2,0)	(3,0)	(4,0)	(0,0)	(1,0)	(2,0)	(3,0)	(4,0)	(0,0)	(1,0)	(2,0)	(3,0)	(4,0)
$ V_{us} $ (central)	0.2211	0.2210	0.2212	0.2228	0.2260	0.2222	0.2224	0.2225	0.2236	0.2253	0.2213	0.2213	0.2219	0.2238	0.2274
m_s	+0.0005 -0.0004	+0.0010 -0.0009	+0.0018 -0.0015	+0.0029 -0.0025	+0.0039 -0.0046	+0.0008 -0.0007	+0.0014 -0.0012	+0.0022 -0.0019	+0.0032 -0.0027	+0.0045 -0.0038	+0.0005 -0.0004	+0.0011 -0.0009	+0.0019 -0.0017	+0.0032 -0.0028	+0.0051 -0.0043
Experimental	+0.0033 -0.0034	+0.0036 -0.0037	+0.0036 -0.0037	+0.0037 -0.0038	+0.0038 -0.0039	+0.0033 -0.0034	+0.0037 -0.0037	+0.0037 -0.0037	+0.0037 -0.0038	+0.0037 -0.0039	+0.0033 -0.0034	+0.0036 -0.0037	+0.0036 -0.0037	+0.0037 -0.0038	+0.0039 -0.0039
Total theory	+0.0005 -0.0005	+0.0010 -0.0010	+0.0020 -0.0020	+0.0036 -0.0037	+0.0062 -0.0065	+0.0009 -0.0009	+0.0019 -0.0019	+0.0033 -0.0033	+0.0051 -0.0050	+0.0074 -0.0071	+0.0005 -0.0004	+0.0011 -0.0010	+0.0022 -0.0020	+0.0040 -0.0036	+0.0068 -0.0061
$s_0 \in [2.5, M_\tau^2]$	0.0030	0.0070	0.0117	0.0188	0.0313	0.0042	0.0089	0.0143	0.0216	0.0325	0.0032	0.0074	0.0126	0.0204	0.0338
total	+0.0045 -0.0045	+0.0080 -0.0080	+0.0124 -0.0124	+0.0195 -0.0196	+0.0321 -0.0322	+0.0054 -0.0054	+0.0098 -0.0099	+0.0151 -0.0151	+0.0225 -0.0225	+0.0336 -0.0335	+0.0046 -0.0047	+0.0084 -0.0084	+0.0133 -0.0133	+0.0211 -0.0211	+0.0347 -0.0346

TABLE XXIII: Determination of $|V_{us}|$ from OPAL data using prescription II. The phenomenological contributions are used for longitudinal components.

-
- [1] M. Davier, A. Hocker and Z. Zhang, Rev. Mod. Phys. **78** (2006), 1043-1109.
- [2] A. Pich, Prog. Part. Nucl. Phys. **75** (2014), 41-85 [arXiv:1310.7922 [hep-ph]].
- [3] K. G. Wilson, Phys. Rev. **179** (1969), 1499-1512
- [4] J. Gasser and H. Leutwyler, Nucl. Phys. B **250** (1985), 465-516
- [5] S. Aoki *et al.* [Flavour Lattice Averaging Group], Eur. Phys. J. C **80** (2020) no.2, 113 [arXiv:1902.08191 [hep-lat]].
- [6] J. L. Kneur and A. Neveu, Phys. Rev. D **101** (2020) no.7, 074009 [arXiv:2001.11670 [hep-ph]].
- [7] J. L. Kneur and A. Neveu, Phys. Rev. D **92** (2015) no.7, 074027 [arXiv:1506.07506 [hep-ph]].
- [8] D. Boito, I. Caprini, M. Golterman, K. Maltman and S. Peris, Phys. Rev. D **97** (2018) no.5, 054007.
- [9] K. G. Chetyrkin, Phys. Lett. B **390** (1997), 309-317 [arXiv:hep-ph/9608318 [hep-ph]].
- [10] C. Becchi, S. Narison, E. de Rafael and F. J. Yndurain, Z. Phys. C **8** (1981), 335
- [11] D. J. Broadhurst, Phys. Lett. B **101** (1981), 423-426
- [12] S. G. Gorishnii, A. L. Kataev, S. A. Larin and L. R. Surguladze, Mod. Phys. Lett. A **5** (1990), 2703-2712
- [13] S. G. Gorishnii, A. L. Kataev, S. A. Larin and L. R. Surguladze, Phys. Rev. D **43** (1991), 1633-1640
- [14] P. A. Baikov, K. G. Chetyrkin and J. H. Kuhn, Phys. Rev. Lett. **96** (2006), 012003 [arXiv:hep-ph/0511063 [hep-ph]].
- [15] E. Gamiz, M. Jamin, A. Pich, J. Prades and F. Schwab, JHEP **01** (2003), 060 [arXiv:hep-ph/0212230 [hep-ph]].
- [16] K. Maltman and J. Kambor, Phys. Rev. D **64** (2001), 093014 [arXiv:hep-ph/0107187 [hep-ph]].
- [17] K. Maltman and J. Kambor, Phys. Rev. D **65** (2002), 074013 [arXiv:hep-ph/0108227 [hep-ph]].

- [18] M. Jamin, J. A. Oller and A. Pich, Nucl. Phys. B **622** (2002), 279-308 [arXiv:hep-ph/0110193 [hep-ph]].
- [19] M. Jamin, J. A. Oller and A. Pich, Eur. Phys. J. C **24** (2002), 237-243 [arXiv:hep-ph/0110194 [hep-ph]].
- [20] B. Ananthanarayan and D. Das, Phys. Rev. D **94**, no. 11, 116014 (2016) [arXiv:1610.08900 [hep-ph]].
- [21] E. Braaten, S. Narison and A. Pich, Nucl. Phys. B **373** (1992), 581-612
- [22] A. Pich and J. Prades, JHEP **10** (1999), 004 [arXiv:hep-ph/9909244 [hep-ph]].
- [23] S. Narison and A. Pich, Phys. Lett. B **211** (1988), 183-188
- [24] F. Le Diberder and A. Pich, Phys. Lett. B **289** (1992), 165-175
- [25] K. Ackerstaff *et al.* [OPAL], Eur. Phys. J. C **7** (1999), 571-593 [arXiv:hep-ex/9808019 [hep-ex]]. Non-strange spectral function is available on link: <https://www.mpp.mpg.de/menke/?q=OPAL>
- [26] M. Davier, A. Höcker, B. Malaescu, C. Z. Yuan and Z. Zhang, Eur. Phys. J. C **74** (2014) no.3, 2803.
- [27] G. Abbiendi *et al.* [OPAL], Eur. Phys. J. C **35** (2004), 437-455 [arXiv:hep-ex/0406007 [hep-ex]].
- [28] D. Boito, M. Golterman, K. Maltman, S. Peris, M. V. Rodrigues and W. Schaaf, Phys. Rev. D **103** (2021) no.3, 034028 [arXiv:2012.10440 [hep-ph]].
- [29] E. Braaten and C. S. Li, Phys. Rev. D **42** (1990), 3888-3891
- [30] J. Erler, Rev. Mex. Fis. **50** (2004), 200-202 [arXiv:hep-ph/0211345 [hep-ph]].
- [31] R. Barate *et al.* [ALEPH], Eur. Phys. J. C **11** (1999), 599-618 [arXiv:hep-ex/9903015 [hep-ex]].
- [32] P.A. Zyla *et al.* [Particle Data Group], PTEP **2020** (2020) no.8, 083C01
- [33] A. H. Hoang, C. Lepenik and V. Mateu, Comput. Phys. Commun. **270** (2022), 108145 [arXiv:2102.01085 [hep-ph]].
- [34] M. R. Ahmady, F. A. Chishtie, V. Elias and T. G. Steele, Phys. Lett. B **479**, 201 (2000) [hep-ph/9910551].
- [35] M. R. Ahmady, F. A. Chishtie, V. Elias, A. H. Fariborz, N. Fattahi, D. G. C. McKeon, T. N. Sherry and T. G. Steele, Phys. Rev. D **66**, 014010 (2002) [hep-ph/0203183].
- [36] M. R. Ahmady, F. A. Chishtie, V. Elias, A. H. Fariborz, D. G. C. McKeon, T. N. Sherry, A. Squires and T. G. Steele, Phys. Rev. D **67**, 034017 (2003) [hep-ph/0208025].
- [37] G. Abbas, B. Ananthanarayan and I. Caprini, Phys. Rev. D **85** (2012) 094018 [arXiv:1202.2672 [hep-ph]].
- [38] B. Ananthanarayan, D. Das and M. S. A. Alam Khan, Phys. Rev. D **102** (2020) no.7, 076008.
- [39] G. Abbas, A. Jain, V. Singh and N. Singh, [arXiv:2205.06061 [hep-ph]].
- [40] T. Appelquist and H. Georgi, Phys. Rev. D **8** (1973), 4000-4002
- [41] A. Zee, Phys. Rev. D **8** (1973), 4038-4041
- [42] K. G. Chetyrkin, A. L. Kataev and F. V. Tkachov, Phys. Lett. B **85** (1979), 277-279
- [43] M. Dine and J. R. Sapiirstein, Phys. Rev. Lett. **43** (1979), 668
- [44] S. G. Gorishnii, A. L. Kataev and S. A. Larin, Phys. Lett. B **259** (1991), 144-150
- [45] L. R. Surguladze and M. A. Samuel, Phys. Rev. Lett. **66** (1991), 560-563 [erratum: Phys. Rev. Lett. **66** (1991), 2416]
- [46] K. G. Chetyrkin, Phys. Lett. B **391** (1997), 402-412 [arXiv:hep-ph/9608480 [hep-ph]].
- [47] P. A. Baikov, K. G. Chetyrkin and J. H. Kuhn, Phys. Rev. Lett. **101** (2008), 012002 [arXiv:0801.1821 [hep-ph]].
- [48] P. A. Baikov, K. G. Chetyrkin and J. H. Kuhn, Phys. Rev. Lett. **104** (2010), 132004 [arXiv:1001.3606 [hep-ph]].
- [49] F. Herzog, B. Ruijl, T. Ueda, J. A. M. Vermaseren and A. Vogt, JHEP **08** (2017), 113
- [50] P. A. Baikov, K. G. Chetyrkin and J. H. Kuhn, Phys. Rev. Lett. **95** (2005), 012003 [arXiv:hep-ph/0412350 [hep-ph]].
- [51] S. C. Generalis, J. Phys. G **15** (1989), L225-L229
- [52] K. G. Chetyrkin and A. Kwiatkowski, Z. Phys. C **59** (1993), 525-532 [arXiv:hep-ph/9805232 [hep-ph]].
- [53] P. A. Baikov, K. G. Chetyrkin and J. H. Kuhn, Nucl. Phys. B Proc. Suppl. **135** (2004), 243-246
- [54] S. G. Gorishnii, A. L. Kataev and S. A. Larin, Nuovo Cim. A **92** (1986), 119-131
- [55] W. Bernreuther and W. Wetzel, Z. Phys. C **11** (1981), 113
- [56] A. Pich and J. Prades, JHEP **06** (1998), 013 [arXiv:hep-ph/9804462 [hep-ph]].
- [57] K. G. Chetyrkin, V. P. Spiridonov and S. G. Gorishnii, Phys. Lett. B **160** (1985), 149-153
- [58] R. M. Albuquerque, S. Narison and M. Nielsen, Phys. Lett. B **684** (2010), 236-245 [arXiv:0904.3717 [hep-ph]].
- [59] H. Leutwyler, NATO Sci. Ser. B **363** (1997), 149-164 [arXiv:hep-ph/9609467 [hep-ph]].
- [60] A. Pich, Prog. Part. Nucl. Phys. **117** (2021), 103846 [arXiv:2012.04716 [hep-ph]].
- [61] M. Beneke and M. Jamin, JHEP **09** (2008), 044.
- [62] S. Chen, M. Davier, E. Gamiz, A. Hocker, A. Pich and J. Prades, Eur. Phys. J. C **22** (2001), 31-38 [arXiv:hep-ph/0105253 [hep-ph]].
- [63] S. Schael *et al.* [ALEPH], Phys. Rept. **421** (2005), 191-284 [arXiv:hep-ex/0506072 [hep-ex]].
- [64] M. Davier, S. Descotes-Genon, A. Hocker, B. Malaescu and Z. Zhang, Eur. Phys. J. C **56** (2008), 305-322 [arXiv:0803.0979 [hep-ph]].
- [65] Y. S. Amhis *et al.* [HFLAV], Eur. Phys. J. C **81** (2021) no.3, 226 [arXiv:1909.12524 [hep-ex]].
- [66] K. Maltman and C. E. Wolfe, Phys. Lett. B **650** (2007), 27-32 [arXiv:hep-ph/0701037 [hep-ph]].
- [67] E. Gamiz, M. Jamin, A. Pich, J. Prades and F. Schwab, Phys. Rev. Lett. **94** (2005), 011803.
- [68] E. Gamiz, M. Jamin, A. Pich, J. Prades and F. Schwab, Nucl. Phys. B Proc. Suppl. **169** (2007), 85-89 [arXiv:hep-ph/0612154 [hep-ph]].
- [69] E. Gamiz, M. Jamin, A. Pich, J. Prades and F. Schwab, Nucl. Phys. B Proc. Suppl. **144** (2005), 59-64 [arXiv:hep-ph/0411278 [hep-ph]].
- [70] E. Gamiz, M. Jamin, A. Pich, J. Prades and F. Schwab, [arXiv:hep-ph/0505122 [hep-ph]].
- [71] L. E. Adam and K. G. Chetyrkin, Phys. Lett. B **329** (1994), 129-135 [arXiv:hep-ph/9404331 [hep-ph]].
- [72] L. V. Lanin, V. P. Spiridonov and K. G. Chetyrkin, Yad. Fiz. **44** (1986), 1372-1374
- [73] D. Boito, D. Hornung and M. Jamin, JHEP **12** (2015), 090 [arXiv:1510.03812 [hep-ph]].
- [74] M. A. Shifman, A. I. Vainshtein and V. I. Zakharov, Nucl. Phys. B **147** (1979), 519-534
- [75] J. Kambor and K. Maltman, Phys. Rev. D **62** (2000),

- 093023 [arXiv:hep-ph/0005156 [hep-ph]].
- [76] K. Maltman and C. E. Wolfe, Phys. Lett. B **639** (2006), 283-289 [arXiv:hep-ph/0603215 [hep-ph]].
- [77] R. J. Hudspith, R. Lewis, K. Maltman and J. Zanotti, Phys. Lett. B **781** (2018), 206-212 [arXiv:1702.01767 [hep-ph]].
- [78] D. J. Gross and F. Wilczek, Phys. Rev. Lett. **30** (1973) 1343.
- [79] W. E. Caswell, Phys. Rev. Lett. **33** (1974) 244.
- [80] D. R. T. Jones, Nucl. Phys. B **75** (1974) 531.
- [81] O. V. Tarasov, A. A. Vladimirov and A. Y. Zharkov, Phys. Lett. **93B** (1980) 429.
- [82] S. A. Larin and J. A. M. Vermaseren, Phys. Lett. B **303** (1993) 334 [hep-ph/9302208].
- [83] T. van Ritbergen, J. A. M. Vermaseren and S. A. Larin, Phys. Lett. B **400** (1997) 379 [hep-ph/9701390].
- [84] M. Czakon, Nucl. Phys. B **710** (2005) 485.
- [85] P. A. Baikov, K. G. Chetyrkin and J. H. Kühn, Phys. Rev. Lett. **118** (2017) no.8, 082002 [arXiv:1606.08659 [hep-ph]].
- [86] F. Herzog, B. Ruijl, T. Ueda, J. Vermaseren and A. Vogt, JHEP **02** (2017), 090 [arXiv:1701.01404 [hep-ph]].
- [87] T. Luthe, A. Maier, P. Marquard and Y. Schröder, JHEP **01** (2017), 081 [arXiv:1612.05512 [hep-ph]].
- [88] R. Tarrach, Nucl. Phys. B **183** (1981), 384-396
- [89] O. V. Tarasov, Phys. Part. Nucl. Lett. **17** (2020) no.2, 109-115 [arXiv:1910.12231 [hep-ph]].
- [90] S. A. Larin, Phys. Lett. B **303** (1993), 113-118.
- [91] J. A. M. Vermaseren, S. A. Larin and T. van Ritbergen, Phys. Lett. B **405** (1997), 327-333 [arXiv:hep-ph/9703284 [hep-ph]].
- [92] K. G. Chetyrkin, Phys. Lett. B **404** (1997), 161-165 [arXiv:hep-ph/9703278 [hep-ph]].
- [93] P. A. Baikov, K. G. Chetyrkin and J. H. Kühn, JHEP **10** (2014), 076 [arXiv:1402.6611 [hep-ph]].
- [94] T. Luthe, A. Maier, P. Marquard and Y. Schröder, JHEP **07** (2016), 127 [arXiv:1606.08662 [hep-ph]].
- [95] P. A. Baikov and K. G. Chetyrkin, PoS **RADCOR2017** (2018), 025
- [96] P. Pascual and E. de Rafael, Z. Phys. C **12** (1982), 127
- [97] M. Jamin and M. Munz, Z. Phys. C **60** (1993), 569-578 [arXiv:hep-ph/9208201 [hep-ph]].
- [98] S. C. Generalis, J. Phys. G **16** (1990), 785-793
- [99] L. R. Surguladze and F. V. Tkachov, Nucl. Phys. B **331** (1990), 35
- [100] E. Bagan, J. I. Latorre and P. Pascual, Z. Phys. C **32** (1986), 43
- [101] D. J. Broadhurst and S. C. Generalis, Phys. Lett. B **165** (1985), 175-180
- [102] S. C. Generalis, J. Phys. G **16** (1990), 367-373
- [103] G. T. Loladze, L. R. Surguladze and F. V. Tkachov, Phys. Lett. B **162** (1985), 363-366